Model of Sarcomeric Ca^{2+} Movements, Including ATP Ca^{2+} Binding and Diffusion, during Activation of Frog Skeletal Muscle

S.M. Baylor and S. Hollingworth

From the Department of Physiology, University of Pennsylvania School of Medicine, Philadelphia, Pennsylvania 19104-6085

ABSTRACT Cannell and Allen (1984. *Biophys. J.* 45:913–925) introduced the use of a multi-compartment model to estimate the time course of spread of calcium ions (Ca^{2+}) within a half sarcomere of a frog skeletal muscle fiber activated by an action potential. Under the assumption that the sites of sarcoplasmic reticulum (SR) Ca^{2+} release are located radially around each myofibril at the Z line, their model calculated the spread of released Ca^{2+} both along and into the half sarcomere. During diffusion, Ca^{2+} was assumed to react with metal-binding sites on parvalbumin (a diffusible Ca^{2+}- and Mg^{2+}-binding protein) as well as with fixed sites on troponin. We have developed a similar model, but with several modifications that reflect current knowledge of the myoplasmic environment and SR Ca^{2+} release. We use a myoplasmic diffusion constant for free Ca^{2+} that is twofold smaller and an SR Ca^{2+} release function in response to an action potential that is threefold briefer than used previously. Additionally, our model includes the effects of Ca^{2+} and Mg^{2+} binding by adenosine 5′-triphosphate (ATP) and the diffusion of Ca^{2+}-bound ATP (CaATP). Under the assumption that the total myoplasmic concentration of ATP is 8 mM and that the amplitude of SR Ca^{2+} release is sufficient to drive the peak change in free [Ca^{2+}] ($\Delta[Ca^{2+}]$) to 18 μM (the approximate spatially averaged value that is observed experimentally), our model calculates that (*a*) the spatially averaged peak increase in [CaATP] is 64 μM; (*b*) the peak saturation of troponin with Ca^{2+} is high along the entire thin filament; and (*c*) the half-width of $\Delta[Ca^{2+}]$ is consistent with that observed experimentally. Without ATP, the calculated half-width of spatially averaged $\Delta[Ca^{2+}]$ is abnormally brief, and troponin saturation away from the release sites is markedly reduced. We conclude that Ca^{2+} binding by ATP and diffusion of CaATP make important contributions to the determination of the amplitude and the time course of $\Delta[Ca^{2+}]$.

KEY WORDS: calcium transients • calcium diffusion • CaATP • ATP diffusion • muscle activation

INTRODUCTION

During normal activation of a skeletal muscle fiber, an action potential in the transverse tubular membranes triggers the opening of Ca^{2+} release channels in the sarcoplasmic reticulum (SR).[1] The released Ca^{2+} produces an increase in the myoplasmic free [Ca] ($\Delta[Ca^{2+}]$), which activates the fiber's contractile response.

The SR calcium release channels ("ryanodine receptors") are found primarily at triadic junctions, where the transverse tubules and the terminal cisternae membranes of the SR are closely apposed. In frog fibers, the triadic junctions are located primarily at the Z lines of the sarcomeres and surround each myofibril with a geometry that approximates an annulus (Peachey, 1965). With this anatomical arrangement, intra-sarcomeric gradients in myoplasmic free [Ca^{2+}] are expected when Ca^{2+} release is active. An understanding of these gradients and the associated movements of Ca^{2+} is important in the interpretation of spatially averaged Ca^{2+} measurements of the type that have been made with a variety of Ca^{2+} indicators. They are also important in the interpretation of local Ca^{2+} measurements of the type that have been made recently with high-affinity indicators and confocal microscopy (Escobar et al., 1994; Tsugorka et al., 1995; Klein et al., 1996).

Cannell and Allen (1984) were the first to use a computer model of a half-sarcomere to estimate the binding and diffusion of Ca^{2+} after its release at the Z line in response to an action potential. A principal motivation was to compare the model predictions about the amplitude and time course of $\Delta[Ca^{2+}]$ with measurements of $\Delta[Ca^{2+}]$ that had been obtained from frog single fibers injected with the indicator aequorin. In this article, we describe a similar computer model developed from a similar motivation. In comparison with Cannell and Allen (1984), our model incorporates three significant differences about the myoplasmic environment and the SR Ca^{2+} release process.

First, we assume a twofold smaller diffusion constant for myoplasmic free Ca^{2+} (3×10^{-6} cm^2 s^{-1} at 16°C vs. 7×10^{-6} cm^2 s^{-1} at 20°C). This difference is based on the

A preliminary account of some of these results was previously published in abstract form (Baylor, S.M., and S. Hollingworth. 1998. *Biophys. J.* 74:A235).

Address correspondence to Dr. S.M. Baylor, Department of Physiology, University of Pennsylvania School of Medicine, Philadelphia, PA 19104-6085. Fax: (215) 573-5851; E-mail: baylor@mail.med.upenn.edu

[1] *Abbreviations used in this paper:* $\Delta[Ca^{2+}]$, free [Ca]; $\Delta[Ca_T]$, the change in total Ca concentration; HFB, hypothetical fixed buffer; PDAA, purpurate-di-acetic acid; SR, sarcoplasmic reticulum.

finding that the viscosity of myoplasm is approximately twofold higher than that of a simple salt solution (Kushmerick and Podolsky, 1969; Maylie et al., 1987*a,b,c*).

Second, the temporal waveform that we assume for SR Ca^{2+} release in response to an action potential (half-width, 1.9 ms at 16°C) is approximately threefold briefer than that assumed by Cannell and Allen (1984) (half-width, 5.8 ms at 20°C). This difference derives from measurements of spatially averaged $\Delta[Ca^{2+}]$ in frog fibers injected with lower-affinity Ca^{2+} indicators such as purpurate-di-acetic acid (PDAA; Southwick and Waggoner, 1989) or furaptra (Raju et al., 1989). These indicators, which appear to track $\Delta[Ca^{2+}]$ in skeletal muscle with 1:1 stoichiometry and little or no kinetic delay (Hirota et al., 1989; Konishi et al., 1991; Zhao et al., 1996), report Ca^{2+} signals that are substantially briefer than estimated with aequorin (Cannell and Allen, 1984). Consequently, estimates of SR Ca^{2+} release with these indicators (Maylie et al., 1987*b*; Baylor and Hollingworth, 1988; Hollingworth et al., 1992, 1996), which to date have been based on spatially averaged models (e.g., Baylor et al., 1983), are substantially briefer than assumed by Cannell and Allen (1984).

Third, we include the reactions of Ca^{2+} and Mg^{2+} with ATP, which is present in the myoplasm of skeletal muscle at millimolar concentration (probably 5–10 mM in a rested fiber; Kushmerick, 1985; Godt and Maughan, 1988; Thompson and Fitts, 1992). Although the fraction of ATP in the Mg^{2+}-bound form (MgATP) at rest is expected to be large (~0.9) at the free $[Mg^{2+}]$ level of myoplasm (see RESULTS), the ATP reaction kinetics (Eigen and Wilkins, 1965) are such that a significant rise in the concentration of Ca^{2+} bound to ATP (Δ[CaATP]) is predicted during activity. Furthermore, ATP is sufficiently small (mol wt, ~500), with an expected myoplasmic diffusion constant of $\sim 1.4 \times 10^{-6}$ $cm^2\ s^{-1}$ at 16°C (Kushmerick and Podolsky, 1969), that a significant transport of Ca^{2+} along the sarcomere in the CaATP form should occur. This transport of Ca^{2+} by CaATP appears to permit a more uniform and synchronous binding of Ca^{2+} to troponin along the thin filament. These effects of ATP in skeletal muscle point to a likely role of ATP in the shaping of local Ca^{2+} gradients in other cells (cf., Zhou and Neher, 1993; Kargacin and Kargacin, 1997).

MATERIALS AND METHODS

Overview of the Multi-compartment Model

Our computational model is similar in principle to that of Cannell and Allen (1984). We divide the myoplasmic space corresponding to a half-sarcomere of one myofibril into a number of compartments that have equal volume and radial symmetry (cf., Fig. 1, where there are six longitudinal by three radial compartments). Within each compartment, appropriate metal-binding sites for Ca^{2+} and Mg^{2+} are included at the total concentrations and with the diffusion constants listed in Table I, *B* and *C* (described below). Resting occupancies of the sites by Ca^{2+} and Mg^{2+} are based on appropriately chosen values of dissociation constants ($K_{d,Ca}$ for Ca^{2+}, $K_{d,Mg}$ for Mg^{2+}) and resting levels of free $[Ca^{2+}]$ and free $[Mg^{2+}]$. The time-dependent calculation is initiated by the introduction of a finite amount of total Ca^{2+}, with an appropriate time course, into the compartment comprising the outermost annulus nearest the Z line (corresponding to the location of the SR release sites; see Fig. 1, *downward arrow*). The calculation is advanced in time by simultaneous integration of the first-order differential

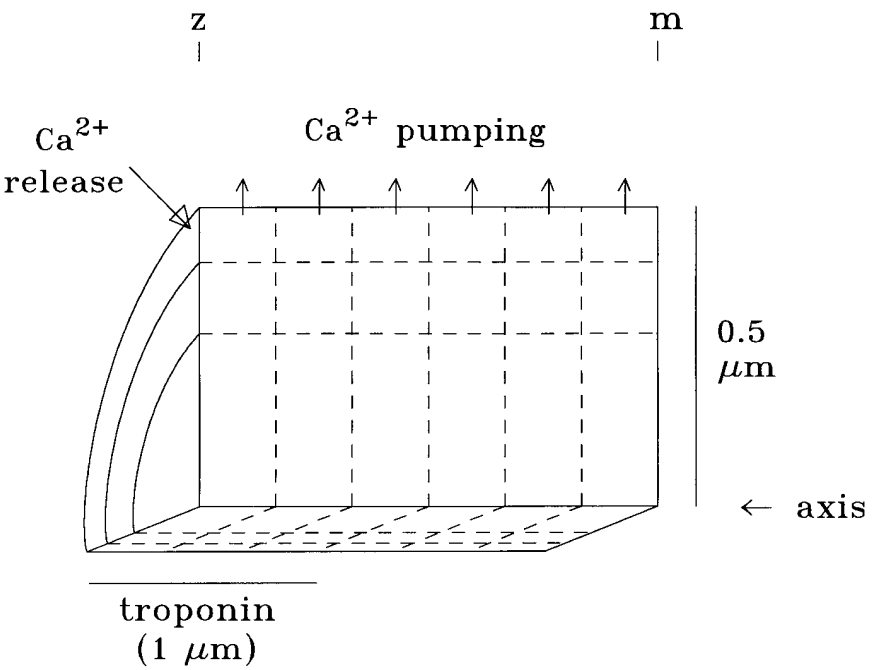

FIGURE 1. Cut-away view of a portion of a half-sarcomere of one myofibril, illustrating the compartment geometry of the model. The fiber axis extends horizontally. As shown here, a typical calculation divides the myoplasm into 18 radially symmetric compartments of equal volume (six axial times three radial). Troponin is assumed to be restricted to the compartments located axially within 1 μm of the Z line (i.e., the length of the thin filaments), whereas the diffusible species (parvalbumin and ATP) are assumed to have access to all compartments. Note that the vertical and horizontal scales are different. See Table I for additional information.

equations for the concentration changes of the various species (free Ca^{2+}; metal-free and metal-bound sites) in all compartments. For the integration, it is assumed that: (*a*) Ca^{2+} and Mg^{2+} react with available binding sites according to the law of mass action; and (*b*) the various species move by the laws of diffusion across any immediately adjacent compartment boundary. Additionally, Mg^{2+} is assumed to be well buffered, so that possible changes in free $[Mg^{2+}]$ are neglected in all compartments.

In each compartment, the binding steps are governed by a mass-action reaction of the type illustrated here for Ca^{2+}:

$$Ca^{2+} + Site \underset{k_{-1}}{\overset{k_{+1}}{\rightleftharpoons}} CaSite.$$

(SCHEME A)

Site and CaSite denote the metal-free and Ca^{2+}-bound forms of the site, respectively, and k_{+1} and k_{-1} denote the on- and off-rate constants, respectively, for the reaction. The corresponding functional form used in the integration is:

$$d[\text{CaSite}]/dt = k_{+1}[Ca^{2+}][\text{Site}] - k_{-1}[\text{CaSite}], \quad (1)$$

where $[Ca^{2+}]$ denotes the free Ca^{2+} concentration ($\Delta[Ca^{2+}]$ + resting $[Ca^{2+}]$). For the sites that bind Mg^{2+} (e.g., parvalbumin; cf., Johnson et al., 1981; Gillis et al., 1982; Baylor et al., 1983), an analogous equation for Mg^{2+} is included in each compartment.

The diffusion of each species across each internal compartment boundary is calculated with an approximation from Fick's law, illustrated here for Ca^{2+}:

$$\text{Flux} = -A \cdot D \cdot \Delta[\text{CaSpecies}]/\Delta x. \quad (2)$$

A denotes the area of the boundary, and *D* denotes the relevant diffusion constant; "CaSpecies" denotes either free Ca^{2+} or one of the Ca^{2+}-binding species listed in Table I; "Δ[CaSpecies]" denotes the difference in species concentration for the two compartments on either side of the boundary being crossed; and Δx denotes the center-to-center distance between the two compartments. The number of boundaries varies from two to four per compartment, according to the compartment's location (see Fig. 1). Ca^{2+}'s spread within the half-sarcomere thus occurs both as diffusion of the free ion and as diffusion of Ca^{2+} bound to mobile sites (parvalbumin, ATP, and indicator but not troponin). For the integration, the number of moles of each species that moves into or out of each compartment per unit time is divided by the compartment volume to determine the effect of diffusion on the change in concentration of that species in that compartment per unit time.

The removal of Ca^{2+} from the half-sarcomere is assumed to take place only from the outermost compartments (see Fig. 1, *upward arrows*). This corresponds to the location of the longitudinal membranes of the SR, which extend from Z line to Z line at the periphery of a myofibril (Peachey, 1965) and contain calcium ATPase molecules (Ca^{2+} pumps) at a high density (Franzini-Armstrong, 1975).

In each compartment, a mass conservation equation is used to track the change in total Ca^{2+} concentration in that compartment (denoted $\Delta[Ca_T]$), equal to the change in compartment Ca^{2+} concentration due to SR release (if any) minus that due to SR pumping (if any) minus the net change in concentrations due to diffusive movements out of the compartment of free Ca^{2+}, Ca^{2+} bound to parvalbumin, and Ca^{2+} bound to ATP. The $\Delta[Ca^{2+}]$ level in each compartment (for use in Eq. 1) is calculated as the $\Delta[Ca_T]$ of the compartment minus the change in compartment concentrations of Ca^{2+} bound to troponin, parvalbumin, and ATP (denoted Δ[CaTrop], Δ[CaParv], and Δ[CaATP], respectively). If the maximum removal rate by the Ca^{2+} pump is set to zero, the mass equations provide a check on the accuracy of the calculation, since the values of $\Delta[Ca_T]$, if summed over all compartments, should then equal the integral of the Ca^{2+} release waveform (Eq. 3, described below) after referral of both quantities to the total myoplasmic volume. This check of the model was satisfied at the level of a fraction of one percent.

Parameters of the Model

Table I *A* gives general information about the model, including the standard dimensions of the half-sarcomere and the most common choice for the number of longitudinal and radial subdivisions. Part B lists the spatial locations of the different metal-binding species and their diffusion constants. In all cases, metal-free and metal-bound diffusion constants are assumed to be identical. The troponin sites are assumed to be fixed because of their attachment to the thin filaments, which in a frog twitch fiber extend 1.0 μm away from the Z line (Page and Huxley, 1963). The other values of the diffusion constants are half those estimated to apply to free solution at 16°C, since the viscosity of myoplasm appears to be about twice that of free solution (Kushmerick and Podolsky, 1969; Maylie et al., 1987*a,b,c*).

Table I *C* lists the assumed concentrations and reaction rate constants for the metal-binding sites on troponin, parvalbumin, and ATP. The values assumed for ATP are explained in the next section. The values for troponin are taken from "model 2" of Baylor et al. (1983), modified slightly as described in Baylor and Hollingworth (1988). The values for parvalbumin are also taken from "model 2" of Baylor et al. (1983), but with two changes. The value for the total concentration of metal sites on parvalbumin is 1,500 rather than 1,000 μM, which reflects a more recent estimate for frog twitch fibers (Hou et al., 1991). The value assumed for the parvalbumin on-rate for Ca^{2+} is threefold smaller than that assumed by Baylor et al. (1983). This latter change is related to our assumption that resting free $[Ca^{2+}]$ is 0.1 μM (cf., Kurebayashi et al., 1993; Harkins et al., 1993; Westerblad and Allen, 1996) rather than the fivefold smaller value assumed by Baylor et al. (1983). There is uncertainty in the values of the parvalbumin reaction rates (Johnson et al., 1981; Ogawa and Tanokura, 1986), and if the Ca^{2+}-parvalbumin on-rate assumed by Baylor et al. (1983) is used, the fraction of the parvalbumin sites bound with Ca^{2+} at a resting $[Ca^{2+}]$ of 0.1 μM is quite large (0.676). This large fraction decreases somewhat the ability of parvalbumin to accelerate the rate of decline of $\Delta[Ca^{2+}]$ after the termination of release. In any event, a threefold variation in the value assumed for the Ca^{2+}-parvalbumin on-rate had only minor effects on the calculations (see RESULTS).

Table I *C* also gives the values of K_d (dissociation constant, calculated as k_{-1}/k_{+1}). Part D lists the fractional occupancies of the metal sites in the resting state, as calculated from the values of K_d and the values assumed for resting $[Ca^{2+}]$ and $[Mg^{2+}]$.

The Reactions of Ca^{2+} and Mg^{2+} with ATP

The competitive reaction of ATP with Ca^{2+} and Mg^{2+} is summarized as follows:

$$Ca^{2+} + ATP \underset{k_{-1}}{\overset{k_{+1}}{\rightleftharpoons}} CaATP,$$

(SCHEME B)

$$Mg^{2+} + ATP \underset{k_{-2}}{\overset{k_{+2}}{\rightleftharpoons}} MgATP,$$

(SCHEME C)

For ATP^{4-}, Eigen and Wilkins (1965) report values of k_{+1} and k_{+2} of $> 10^9$ M^{-1} s^{-1} and 1.3×10^7 M^{-1} s^{-1}, respectively (25°C; ionic strength, 0.1–0.2 M), whereas under similar conditions the values of $K_{d,Ca}$ ($= k_{-1}/k_{+1}$) and $K_{d,Mg}$ ($= k_{-2}/k_{+2}$) are approximately 60 μM and 30 μM, respectively (Botts et al., 1965; Phillips et al., 1966). Thus, k_{-1} and k_{-2} are calculated to be >60,000 s^{-1} and 390 s^{-1}, respectively. At 16°C and a viscosity of 2 cP (i.e., appropriate to the model conditions), reaction rates would be smaller, with k_{-1} and k_{-2} values of perhaps 30,000 s^{-1} and 150 s^{-1}, respectively. Moreover, at the pH (~7) and K^+ concentration (~140 mM) of myoplasm, the effective values of $K_{d,Ca}$ and $K_{d,Mg}$ are elevated because of partial binding of K^+ and H^+ to ATP^{4-}. Under these conditions, we estimate that $K_{d,Ca}$ and $K_{d,Mg}$ are ~200 and ~100 μM, respectively (Botts et al., 1965; Phillips et al., 1966; Martell and Smith, 1974). Thus, in the model, the values assumed for k_{+1} ($= k_{-1}/K_d$) and k_{+2} ($= k_{-2}/K_d$) are 1.5×10^8 M^{-1} s^{-1} and 1.5×10^6 M^{-1} s^{-1}, respectively.

Given these reaction rates, single-compartment (i.e., spatially homogeneous) calculations were carried out to estimate the kinetic response of the ATP reactions if driven by a substantial Ca^{2+} transient. The total concentration of ATP was assumed to be 8 mM, a value near the middle of the range of values recently reported

TABLE I

Parameters of the Standard Multi-compartment Model

A. General

Temperature	16°C
Length, z- to m-line	2.0 μm
Length of thin filament	1.0 μm
Radius of myofibril	0.5 μm
Resting free [Ca^{2+}]	0.1 μM
Resting free [Mg^{2+}]	1.0 mM
Longitudinal subdivisions	6
Radial subdivisions	3

B. Spatial Distributions and Diffusion Constants

Species	Location	Diffusion constant
		10^{-6} cm^2 s^{-1}
Free Ca^{2+}	All compartments	3
Troponin	Compartments within 1.0 μm of the z-line	0
Parvalbumin	All compartments	0.15
ATP	All compartments	1.4
Indicator dyes	All compartments	0.20–0.99

C. Bulk Concentrations and Ca^{2+} and Mg^{2+} Reaction Rates

Species	[Total sites]	k_{+1}	k_{-1}	K_d
	μM	*10^8 M^{-1} s^{-1}*	*s^{-1}*	*μM*
Troponin (regulatory)	240	0.885	115	1.3
Parvalbumin	1,500			
Ca^{2+}		0.417	0.5	0.012
Mg^{2+}		0.00033	3.0	91.0
ATP	8,000	0.1364*	30,000*	2,200*

D. Resting Fractional Occupancies of Sites by Ca^{2+} and Mg^{2+}

	Ca^{2+}	Mg^{2+}
Troponin (regulatory)	0.071	—
Parvalbumin	0.410	0.541
ATP	0.000	0.909*

The table lists general information as well as typical values used for the model calculations. In *B*, all species are assumed to diffuse in myoplasm except for troponin, which is fixed at the location of the thin filament. In *C*, the site concentrations are referred to the myoplasmic water volume (cf., Baylor et al., 1983); the values of k_{+1}, k_{-1}, and K_d ($= k_{-1}/k_{+1}$) are for Ca^{2+} unless indicated otherwise. The asterisk in *C* and *D* denotes that the rates for Ca^{2+}-ATP are effective rates in the presence of 1 mM free [Mg^{2+}] and that a reduced set of equations involving the effective occupancy of ATP with Mg^{2+} was used for the majority of calculations with ATP included (see MATERIALS AND METHODS).

for fast-twitch fibers, 5–10 mM (Kushmerick, 1985; Godt and Maughan, 1988; Thompson and Fitts, 1992). (Note: As for the other species of this article, the ATP concentration is referred to the myoplasmic water volume; see Baylor et al., 1983; Godt and Maughan, 1988.) The free $[Mg^{2+}]$ was assumed to be 1 mM and constant.

Fig. 2 shows the responses of Schemes B and C if driven simultaneously by a $\Delta[Ca^{2+}]$ of peak amplitude 18.0 μM, a time-to-peak of 2.90 ms, and half-width of 5.90 ms, i.e., similar to that expected for the spatially averaged $\Delta[Ca^{2+}]$ of a single myofibril (see RESULTS). The Δ[CaATP] response (upper trace) has a time-to-peak of 2.98 ms and a half-width of 6.09 ms; as a waveform, it is virtually indistinguishable from that of $\Delta[Ca^{2+}]$ (not shown). The amplitude of Δ[CaATP], however, at 63.9 μM, is 3.6-fold larger than that of $\Delta[Ca^{2+}]$. The factor 3.6 comes from the ratio of total [ATP] (8 mM) to the effective value of $K_{d,Ca}$ in the presence of 1 mM free $[Mg^{2+}]$ (2.2 mM = the actual $K_{d,Ca}$ of 200 μM times the factor $\{1 + [Mg^{2+}]/K_{d,Mg}\}$; see Scheme B). Fig. 2 shows that, on a millisecond time scale, ATP behaves as a rapid and linear Ca^{2+} buffer, with the concentration of Ca^{2+} bound to ATP being nearly fourfold larger than that of free $[Ca^{2+}]$.

The lower trace in Fig. 2 shows the Δ[MgATP] response for the same calculation; the peak change is −53.4 μM. With a time-to-peak of 3.73 ms and half-width of 6.96 ms, the Δ[MgATP] waveform also closely tracks $\Delta[Ca^{2+}]$, although not quite as faithfully as does Δ[CaATP]. Because ATP transiently releases ~53 μM total Mg^{2+}, an increase in free $[Mg^{2+}]$ would occur if the solution were not well buffered for Mg^{2+}. In the case of myoplasm, any Mg^{2+} released by ATP would be buffered by phospho-creatine (primarily), which would limit the increase in free $[Mg^{2+}]$ to about one-third the increase in total $[Mg^{2+}]$ (e.g., Baylor et al., 1985). Thus, in myoplasm, spatially averaged free $[Mg^{2+}]$ would remain nearly constant, rising by only ~2% relative to the resting level of 1 mM.

Since the Δ[CaATP] response in Fig. 2 is fast and linear and the implied increase in myoplasmic free $[Mg^{2+}]$ is small, the Δ[CaATP] response can be closely approximated by an equivalent reaction (termed here the "reduced" reaction), which omits consideration of Δ[MgATP]:

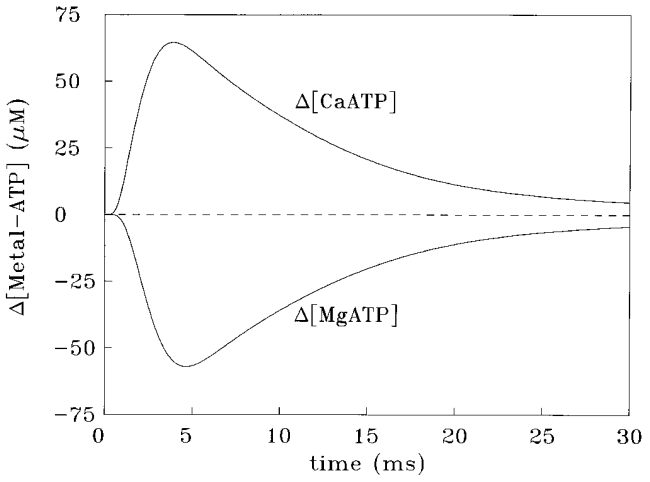

FIGURE 2. Single-compartment simulation of the response of 8 mM total ATP to a $[Ca^{2+}]$ transient of peak amplitude 18.0 μM, time-to-peak 2.90 ms, and half-width 5.90 ms. Schemes B and C were simulated with the Ca^{2+} and Mg^{2+} reaction rates given in the text; free $[Mg^{2+}]$ was 1 mM and constant.

$$Ca^{2+} + ATP \underset{k_{-1}}{\overset{k'_{+1}}{\rightleftharpoons}} CaATP.$$

(SCHEME D)

For this reaction, it is assumed that k_{-1} has the same value as does Scheme B, but that k'_{+1} is 11-fold smaller than k_{+1}, 1.36×10^7 M^{-1} s^{-1} ($= 1.5 \times 10^8$ M^{-1} $s^{-1}/11$). This decrease reflects the assumption that resting free $[Mg^{2+}]$ is 1 mM (10-fold higher than $K_{d,Mg}$), which reduces by 11-fold the fraction of total ATP that is immediately available to react with Ca^{2+}. Thus, the 11-fold reduction in k_{+1} accounts for the 11-fold increase in effective value of $K_{d,Ca}$ due to 1 mM $[Mg^{2+}]$. The response of Scheme D to the same $\Delta[Ca^{2+}]$ driving function used for Fig. 2 was also calculated (not shown). As expected, this Δ[CaATP] response was virtually identical to that of Δ[CaATP] shown in Fig. 2; it had a peak amplitude of 64.9 μM, a time-to-peak of 2.93 ms, and a half-width of 5.94 ms (vs. 63.9 μM, 2.98 ms and 6.09 ms, respectively, for Δ[CaATP] in Fig. 2). Thus, the reduced reaction (Scheme D), which speeds and simplifies the calculations of Δ[CaATP] in the multi-compartment model, closely approximates the complete reaction system (Schemes B and C). Although it is possible that other constituents of myoplasm might also bind significant concentrations of Ca^{2+}, our examination of the list of constituents for frog myoplasm (Godt and Maughan, 1988) indicates that ATP is the major (known) species that, to date, has not been included in kinetic models of Ca^{2+} binding in skeletal muscle. Phospho-creatine, although present in resting fibers at a concentration that is approximately four times larger than that of ATP, has, in the presence of 1 mM free $[Mg^{2+}]$, an effective value of $K_{d,Ca}$ that is about 16-fold larger (36 mM vs. 2.2 mM) (cf., Smith and Alberty, 1956; O'Sullivan and Perrin, 1964; Sillen and Martell, 1964). Thus, the ability of phospho-creatine to act as a Ca^{2+} buffer is expected to be only ~25% of that of ATP. For other compounds that are present at millimolar or near millimolar concentrations in myoplasm, e.g., inorganic phosphate and carnosine, the Ca^{2+} buffering effect is expected to be no more than a few percent of that of ATP (Sillen and Martell, 1964; Lenz and Martell, 1964; Godt and Maughan, 1988).

Ca^{2+} Release from the SR

The form of the equation assumed in the multi-compartment model for SR Ca^{2+} release in response to an action potential is

$$\text{Release Rate} = R[1 - \exp(-t/\tau_1)]^L \cdot [\exp(-t/\tau_2)]^M. \quad (3)$$

Release rate has units of micromoles of Ca^{2+} per liter of myoplasmic water per millisecond (μM/ms) and its time course, in the absence of SR Ca^{2+} depletion, reflects the open time of the SR Ca^{2+}-release channels. The choice of a product of exponentials, as given on the right-hand side of Eq. 3, is empirical. The values selected for τ_1, τ_2, L, and M (1.5 ms, 1.9 ms, 5 and 3, respectively) give a waveform of SR Ca^{2+} release that is similar to the release waveform estimated with our single-compartment model when driven with experimental measurements of $\Delta[Ca^{2+}]$ (see RESULTS). With these selections, the time-to-peak and half-width of the release rate are 1.70 and 1.93 ms, respectively. The value chosen for R varied with the particular model being examined (see RESULTS) but was usually adjusted so that the peak of spatially averaged $\Delta[Ca^{2+}]$ would be 18 μM, the value expected from the ex-

perimental measurements (cf., the first section of RESULTS). For the standard multi-compartment calculation with ATP (cf., Fig. 4), the value of R corresponds to a peak release rate of 141 μM/ms. The corresponding spatially averaged total concentration of released Ca^{2+}, which is given by the integral of release rate with respect to time, is 296 μM.

Ca^{2+} Uptake by the SR

The form of the equation assumed for Ca^{2+} uptake from the half-sarcomere by the SR Ca^{2+} pump is

$$\text{Pump Rate} = -P[1-\exp(-t/\tau)]^N \cdot [Ca^{2+}]^2/([Ca^{2+}]^2 + (K_d)^2). \quad (4)$$

The minus sign signifies that Ca^{2+} is removed from the myoplasm, and P gives the maximum removal rate (units of μM/ms). The choice of functional form for the remaining terms reflects the relatively short time scale of the calculations (≤30 ms) and is largely empirical. With τ and N chosen to be 1 ms and 10, respectively, the exponential term gives a small delay (2–3 ms) for pump activation after initiation of the calculation. The introduction of this delay, while somewhat arbitrary, permits the initial binding of Ca^{2+} by troponin to precede the initial pumping of Ca^{2+} by the SR Ca^{2+} pump. With the parameter P selected to be 1.5 μM/ms (concentration referred to the entire half-sarcomere) and with K_d selected to be 1 μM, the return of spatially averaged $\Delta[Ca^{2+}]$ towards baseline at later times in the calculation (10–30 ms) is similar to that observed experimentally (cf., Figs. 3 and 4 *A* of RESULTS). Although it is possible in principle to include a reaction mechanism for the pump that explicitly calculates the concentration of Ca^{2+} bound by the pump (e.g., the 11-state cycle of Fernandez-Belda et al., 1984—for example, as implemented by Pape et al., 1990, in their single-compartment model), this approach was deemed too complicated and very unlikely to change the main conclusions of this article. As an additional simplification, the resting removal of Ca^{2+} by the SR Ca^{2+} pump and the resting leak of Ca^{2+} through the efflux channels were assumed to be zero.

Implementation

Calculations and figure preparation were carried out on a DOS platform (100 MHz Pentium computer) with programs written in MLAB (Civilized Software, Bethesda, MD), a high-level language for differential equation solving, curve fitting, and graphics. In the 18-compartment model with ATP included, the total number of differential equations requiring simultaneous solution is ~100. This number is close to the maximum possible number of such equations that the 1997 DOS version of MLAB can handle. Because of this constraint, the "reduced" reaction of Ca^{2+} with ATP (Scheme D) was used in the multi-compartment calculations with ATP included.

Single Fiber Measurements

Intact single twitch fibers of semi-tendinosus or iliofibularis muscles of *Rana temporaria* were isolated and pressure injected with furaptra. The indicator concentration in myoplasm was sufficiently small (<0.2 mM) that the fiber's $\Delta[Ca^{2+}]$ signal in response to action potential stimulation was not altered significantly by the indicator. The furaptra fluorescence signal was measured and calibrated as described previously (Konishi et al., 1991; Zhao et al., 1996).

RESULTS

Summary of Experimental Features of $\Delta[Ca^{2+}]$ in Response to an Action Potential

Our previous experiments that measured spatially averaged $\Delta[Ca^{2+}]$ in response to an action potential (16°C) provide an important constraint for the evaluation of the multi-compartment model of this article. Most of these experiments used intact frog twitch fibers of typical diameter (~90 μm) and used furaptra, a lower-affinity, rapidly reacting fluorescence indicator (Konishi et al., 1991; Hollingworth et al., 1996; Zhao et al., 1996). However, any attempt to relate the properties of the furaptra fluorescence measurements to the $\Delta[Ca^{2+}]$ of a single myofibril involves several complications.

First, the myoplasmic value of furaptra's $K_{d,Ca}$ is uncertain. Our calibration of the furaptra fluorescence signal uses a $K_{d,Ca}$ of 98 μM (16°C), which is the value obtained from a comparison of the furaptra measurements with the $\Delta[Ca^{2+}]$ signal from PDAA (Konishi and Baylor, 1991; Konishi et al., 1991). Because PDAA is a rapidly reacting Ca^{2+} indicator of low-affinity ($K_{d,Ca} \approx$ 1 mM) and does not bind strongly to myoplasmic constituents, PDAA is thought to give the most reliable available estimate of $\Delta[Ca^{2+}]$ (Hirota et al., 1989). The value of 98 μM for furaptra's myoplasmic $K_{d,Ca}$ is about twofold higher than the 49 μM value estimated for the indicator in a salt solution (16°C, free $[Mg^{2+}]$ = 1 mM); an increased value is expected in myoplasm because of the binding of furaptra to myoplasmic constituents (Konishi et al., 1991). From the average experimental value in frog fibers (0.144) observed for the peak of furaptra's Δf_{CaD} signal (the change in the fraction of indicator in the Ca^{2+}-bound form due to an action potential), the average value calibrated for the peak of $\Delta[Ca^{2+}]$ is 16.5 μM (Hollingworth et al., 1996; Zhao et al., 1996). From the same measurements, the average values estimated for time-to-peak and half-width of $\Delta[Ca^{2+}]$ are 5.0 and 9.6 ms, respectively.

Second, as noted by Konishi et al. (1991), who made simultaneous measurements of $\Delta[Ca^{2+}]$ with PDAA and furaptra from the same region of the same fiber, the furaptra measurements may overestimate slightly the actual values for the time-to-peak and half-width of $\Delta[Ca^{2+}]$. This follows because the time-to-peak and half-width values measured with PDAA were slightly briefer (by about 0.3 and 1.5 ms, respectively) than the furaptra measurements.

Third, as noted by Hollingworth et al. (1996), a slightly larger and briefer $\Delta[Ca^{2+}]$ signal is found in experiments with smaller-diameter frog fibers. In four such fibers (diameters 45–54 μm), the average furaptra $\Delta[Ca^{2+}]$ values were 17.3 μM for peak, 4.4 ms for time-to-peak, and 8.2 ms for half-width (compared with 16.5 μM, 5.0 and 9.6 ms, respectively, for ordinary-sized fi-

bers—mentioned above). These differences presumably arise because delays associated with radial propagation of the tubular action potential (Adrian and Peachey, 1973; Nakajima and Gilai, 1980) are smaller in smaller diameter fibers. Thus, the dispersive effects on the spatially averaged $\Delta[Ca^{2+}]$ signal due to nonsynchronous activation of individual myofibrils should be smaller. We assume that if measurements could be made in the absence of any radial delays, $\Delta[Ca^{2+}]$ would be slightly larger and briefer.

Based on these considerations, we expect that the following approximate values should apply to $\Delta[Ca^{2+}]$ of a single myofibril at 16°C: peak amplitude, ~18 μM; time-to-peak, ~4 ms; half-width, ~6 ms. In the absence of longitudinal propagation delays (appropriate for the multi-compartment model), the value for time-to-peak is expected to be ~3 ms.

Summary of Estimates of SR Ca^{2+} Release Obtained with the Single-compartment Model

The furaptra $\Delta[Ca^{2+}]$ measurements can be used as input to the single compartment model of Baylor et al. (1983) to estimate the amplitude and time course of SR Ca^{2+} release (e.g., Hollingworth et al., 1996). With this model, it is assumed that myoplasmic changes occur uniformly in space and that the change in total myoplasmic Ca^{2+} concentration due to SR release ($\Delta[Ca_T]$) can be estimated from the summed changes of Ca^{2+} in four pools: (*a*) Δ[CaD] (the change in concentration of Ca^{2+} bound to furaptra, which can be directly calibrated from the measured change in indicator fluorescence, Δ*F*), (*b*) $\Delta[Ca^{2+}]$ itself (calibrated as described in the previous section), (*c*) Δ[CaTrop], and (*d*) Δ[CaParv]. Given $\Delta[Ca^{2+}]$ and the assumed resting $[Ca^{2+}]$ of 0.1 μM, changes *c* and *d* can be calculated from Eq. 1 (described in MATERIALS AND METHODS) and the reaction parameters given in Table I *C*.

Fig. 3 shows an example of this model applied to measurements from a frog fiber of small diameter (45 μm). The four lower traces show the estimated changes in Ca^{2+} concentration in the four pools described in the preceding paragraph. The next trace (*Δ[CaATP]*) shows the estimated concentration change in a fifth pool, that of Ca^{2+} bound to ATP (cf., Fig. 2). Two $\Delta[Ca_T]$ traces were computed (not shown). The first, which equaled the sum of the concentration changes in the original four pools, had a peak value of 291 μM and a time-to-peak of 6.5 ms; the second, which also included the contribution of Δ[CaATP], had a peak value of 339 μM and a time-to-peak of 5.5 ms. The two traces at the top of Fig. 3 show the time derivative ($d\Delta[Ca_T]/dt$) of the two $\Delta[Ca_T]$ signals; these traces supply two estimates of the net flux of Ca^{2+} between SR and myoplasm (i.e., release rate minus uptake rate). The large early positive deflections essentially reflect the release process. The effect of Ca^{2+} uptake is apparent only at later times when, with the cessation of release, the traces go slightly negative. The smaller of the two $d\Delta[Ca_T]/dt$ signals (*second from top*) had a peak

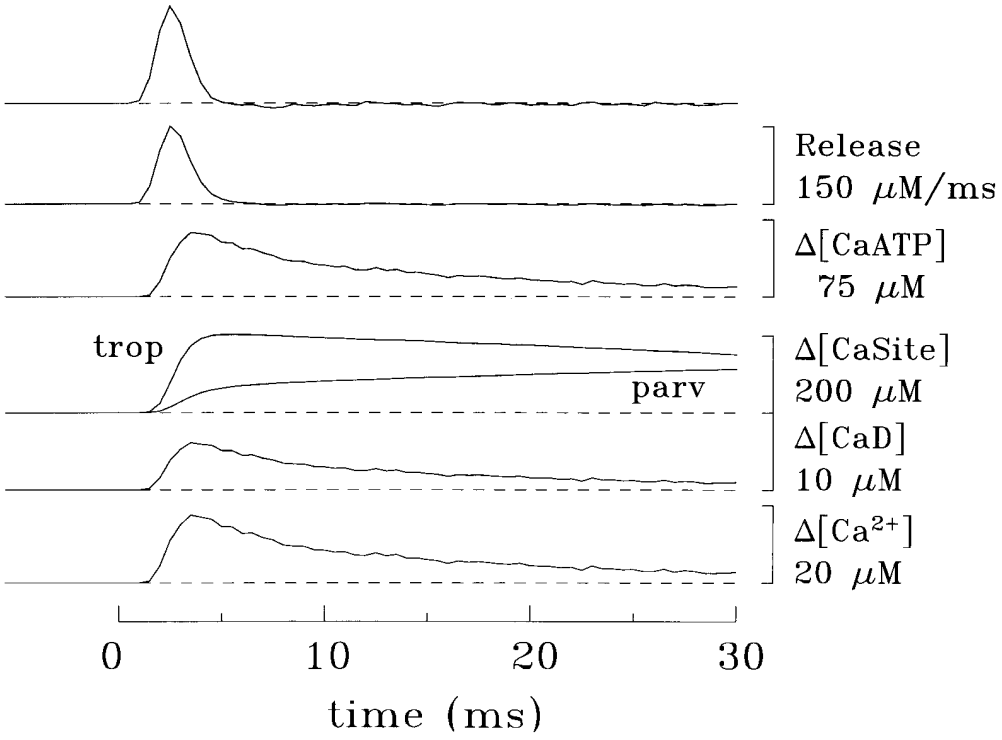

FIGURE 3. Example of the single-compartment model of Baylor et al. (1983) to estimate SR Ca^{2+} release (*top two traces*, referred to in the text as the $d\Delta[Ca_T]/dt$ signal); the uppermost calibration bar applies to both traces. The furaptra Δ[CaD] signal (*second trace from the bottom*) was measured in a frog fiber of small diameter (45 μm). $\Delta[Ca^{2+}]$ (*bottom trace*) was estimated from the furaptra signal by the single-compartment method described in the text and used to calculate the Δ[CaTrop], Δ[CaParv],] and Δ[CaATP] responses. Fiber reference, 032896.2; sarcomere length, 3.8 μm; 16°C; furaptra concentration, 0.04 mM.

value of 146 μM/ms, a time-to-peak of 2.5 ms, and a half-width of 1.8 ms, whereas the larger signal (*top*), which includes the contribution of Δ[CaATP], had a peak value of 183 μM/ms, a time-to-peak of 2.5 ms, and a half-width of 1.8 ms.

Results similar to those in Fig. 3 were observed in a total of four small-diameter frog experiments. Without inclusion of ATP, the average values (±SEM) estimated for the $\Delta[Ca_T]$ signal were 298 ± 4 μM for peak amplitude and 6.5 ± 0.1 ms for time-to-peak; with inclusion of ATP, the values were 351 ± 9 μM and 5.6 ± 0.1 ms, respectively. For the $d\Delta[Ca_T]/dt$ signal, the average values without inclusion of ATP were 142 ± 4 μM/ms for peak amplitude, 2.9 ± 0.2 ms for time-to-peak, and 1.9 ± 0.1 ms for half-width; with ATP, the values were 176 ± 7 μM/ms, 2.9 ± 0.2 ms, and 1.9 ± 0.1 ms, respectively. All values for time-to-peak likely include a small delay, ~1 ms, because of action potential propagation.

These calculations indicate that the inclusion of ATP, with properties as specified in Table I, in the single-compartment model of Baylor et al. (1983) increases the estimated peak value of $\Delta[Ca_T]$ by about 53 μM (18%) and that of $d\Delta[Ca_T]/dt$ by about 34 μM/ms (24%). Interestingly, these changes occur with very little change in the main time course of the $d\Delta[Ca_T]/dt$ signal, as the estimates for time-to-peak and half-width of release were unaltered. This finding supports the use of the SR Ca^{2+} release function described in MATERIALS AND METHODS (Eq. 3) as the starting point for the calculations with the multi-compartment model.

Results of the Multi-compartment Model without Inclusion of ATP

At the outset, it is useful to note two important conceptual differences between single- and multi-compartment modeling. First, with a single-compartment model, calculations can be applied in either of two logical directions: (*a*) backward, from $\Delta[Ca^{2+}]$ to a release waveform (e.g., as in Fig. 3) or (*b*) forward, from the release waveform to $\Delta[Ca^{2+}]$ (not shown). In contrast, with the multi-compartment approach, only calculations in the forward direction are practical because spatially averaged $\Delta[Ca^{2+}]$ results from the summed changes in a number of different compartments (e.g., 18 as in Fig. 1). The procedure adopted for the multi-compartment calculations was thus to assume an SR Ca^{2+} release waveform as driving function and evaluate its success by a comparison of calculated spatially averaged $\Delta[Ca^{2+}]$ with expectations from the measurements of $\Delta[Ca^{2+}]$ (cf., first section of RESULTS). This evaluation compared values for peak amplitude, time-to-peak, and half-width of $\Delta[Ca^{2+}]$. Secondly, only the multi-compartment model calculates concentrations as a function of spatial location. Thus, single-compartment calculations are expected to have errors associated with an inability to estimate local gradients in $\Delta[Ca^{2+}]$ and the associated gradients in Ca^{2+} bound to nonlinear (saturable) binding sites. In consequence, inconsistencies are expected to arise between single- and multi-compartment calculations with otherwise identical parameters.

The first calculations with the multi-compartment model did not include ATP and provide a useful baseline for assessment of the effect of the inclusion of ATP (next section). The amplitude initially selected for the parameter R in the release waveform driving function (Eq. 3) corresponds to a spatially averaged release rate of 142 μM/ms, the value estimated from the single-compartment model without ATP (preceding section). A striking result of this calculation (not shown) is that spatially averaged $\Delta[Ca^{2+}]$ is very different from the expectations outlined in the first section of RESULTS. Its peak amplitude, 58 μM, is about threefold larger than expected (~18 μM), and its half-width, 3.6 ms, is markedly briefer than expected (~6 ms). The time-to-peak (3.2 ms), however, is close to expected (~3 ms). This large discrepancy between the single- and multi-compartment results has two possible sources. First, there might be a significant error in the $d\Delta[Ca_T]/dt$ signal used to drive the multi-compartment model, in which case the effect of other parameter selections (including the omission of ATP) becomes difficult to evaluate. Alternatively, the $d\Delta[Ca_T]/dt$ signal may be approximately correct, in which case the omission of ATP and/or the choice of the other model parameters must be quite significant.

Although it is possible that the $d\Delta[Ca_T]/dt$ signal, which is based on the single-compartment model, may have errors in both amplitude and time course, other experimental evidence supports the conclusion that the time course of the $d\Delta[Ca_T]/dt$ signal is approximately correct. This evidence comes from action potential experiments on fibers that contained millimolar concentrations of a high-affinity Ca^{2+} buffer such as fura-2 (Baylor and Hollingworth, 1988; Hollingworth et al., 1992; Pape et al., 1993) or EGTA (Jong et al., 1995). At millimolar concentrations, these buffers rapidly bind most of the Ca^{2+} that is released from the SR, and thus their optical signal, which is proportional to the amount of bound Ca^{2+}, closely tracks $\Delta[Ca_T]$. The time derivative of this signal had a half-width of ~3 ms. Although this value is ~1 ms larger than that of the $d\Delta[Ca_T]/dt$ waveform defined by Eq. 3, a larger experimental half-width is expected for two reasons. First, the fibers of these experiments were of typical diameter (~90 μm) rather than small diameter. Second, because the myoplasmic $\Delta[Ca^{2+}]$ signal in these fibers was reduced and abbreviated (due to the presence of millimolar Ca^{2+} buffer), there was likely relief from the process of Ca^{2+}-inactivation of SR Ca^{2+} release (Baylor et al.,

1983; Schneider and Simon, 1988). This process normally serves to abbreviate the time course of SR release.

Given this support for the time-dependent part of Eq. 3, it was of interest to redo the multi-compartment calculation described above with the amplitude factor R reduced so that the peak value of spatially averaged $\Delta[Ca^{2+}]$ would be 18 μM, the value expected from the experimental measurements (cf., first section of RESULTS). To achieve this result, an R value of 89 μM/ms is required (instead of 142 μM/ms). In this case, however, the half-width of $\Delta[Ca^{2+}]$ is only 2.6 ms, which is even briefer than calculated initially (3.6 ms) and less than half the expected value (~6 ms). In summary, because these calculations failed to produce a spatially averaged $\Delta[Ca^{2+}]$ that is acceptable in both amplitude and time course, the multi-compartment model appears to have some important error or omission unrelated to the use of Eq. 3 as driving function.

Results of the Multi-compartment Model with Inclusion of ATP

The next calculations included ATP, with the value of R set initially to 176 μM/ms (the value estimated from the single-compartment model with ATP; see second section of RESULTS). In this case, spatially averaged $\Delta[Ca^{2+}]$ (not shown) has a peak value of 27.7 μM and a half-width of 10.6 ms. Both values are substantially larger than expected from the measurements (~18 μM peak and ~6 ms half-width) and again imply some significant error or omission.

As in the preceding section, the multi-compartment calculation with ATP was then repeated but with the value of R lowered (to 141 μM/ms) so as to yield an amplitude of 18 μM for spatially averaged $\Delta[Ca^{2+}]$. The results of this calculation are shown in Fig. 4. Interestingly, spatially averaged $\Delta[Ca^{2+}]$ (Fig. 4 *A*) has values for time-to-peak and half-width of 3.2 and 5.2 ms, respectively, which are quite close to the expected values (~3 and ~6 ms, respectively).

Fig. 4 *B* shows the associated calculations of Δ[CaTrop], which involve nine troponin-containing compartments. For Δ[CaTrop], a value of 446 μM on the ordinate corresponds to 100% occupancy of the troponin sites with Ca^{2+}. (The 446 μM value is calculated from the 240 μM value given in Table I *C* times a factor of two [since the troponin sites are located in only half of the compartments in Fig. 1] minus the resting occupancy of tropo-

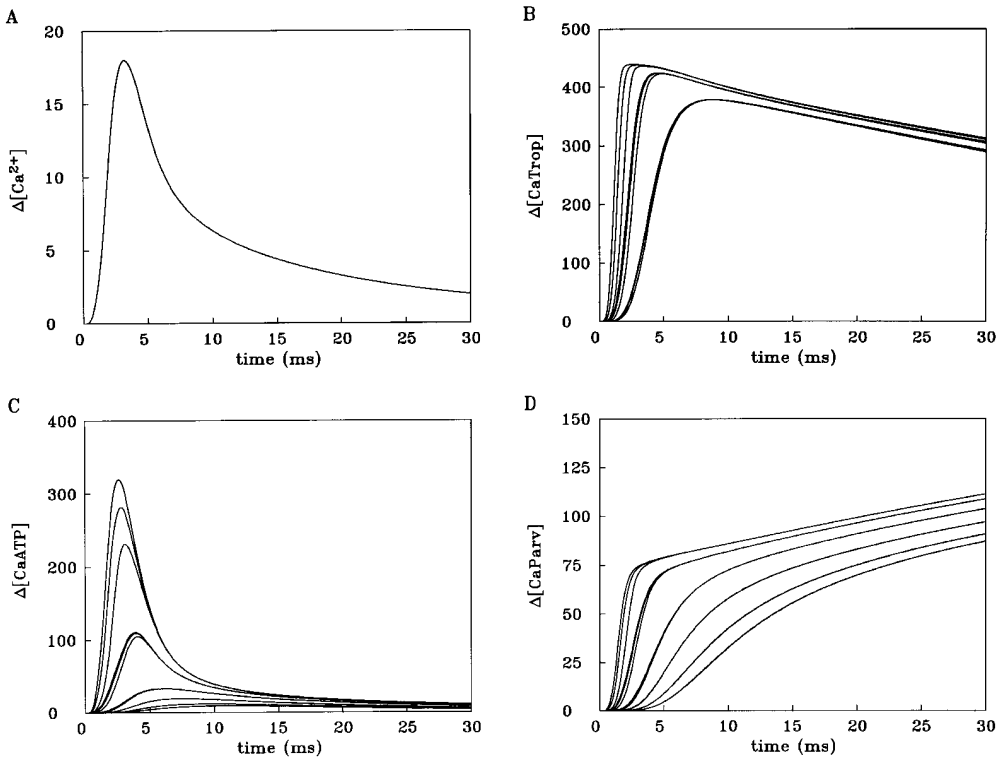

FIGURE 4. 18-compartment calculation with ATP included. *A* shows spatially averaged $\Delta[Ca^{2+}]$. *B* shows the Δ[CaTrop] responses for the nine compartments that contain troponin; a value of 446 μM on the ordinate corresponds to 100% occupancy of troponin with Ca^{2+}. The three largest Δ[CaTrop] changes are from the three radial compartments adjacent to the Z line. Among these three, the peak rate of rise progressively decreases from edge to middle to center of the myofibril. A similar progression is seen for the three Δ[CaTrop] changes of intermediate size (which correspond to the middle third of the thin filament) and for the three smallest Δ[CaTrop] changes (which correspond to the thin filament regions most distant from the Z line). *C* shows the 18 individual Δ[CaATP] responses. Their amplitudes decrease progressively in a manner analogous to that described in *B*. Only the three largest Δ[CaATP] responses (from the three radial compartments adjacent to the Z line) are well resolved individually; for the other changes, the radial gradient is almost negligible, and thus, at the display gain shown, traces for the radial compartments at other axial locations are indistinguishable. *D* shows the 18 individual Δ[CaParv] changes, again with an analogous progression in amplitudes. The amplitude of the SR Ca^{2+} release function (cf., Eq. 3) was 141 μM/ms if referred to the myoplasmic volume of the half-sarcomere. See Table I for a summary of other model parameters.

nin with Ca^{2+}, 34 μM [= 0.071 × 480 μM; cf., Table I *D*].) In all nine compartments, the occupancy of troponin with Ca^{2+} reached a peak level that is close to saturation (>85%). Thus, the underlying Ca^{2+} transients in the troponin-containing compartments are of sufficient amplitude and duration to give nearly complete activation of troponin along the entire thin filament, as expected from fiber mechanical measurements (e.g., Gordon et al., 1964).

Fig. 4, *C* and *D*, shows the calculations of Δ[CaATP] and Δ[CaParv], respectively, in the 18 compartments. The calculations of Δ[Ca^{2+}] for the individual compartments are not shown, but the time course and relative amplitude of these changes are closely similar to those shown in Fig. 4 *C* for Δ[CaATP]. This follows because (*a*) as mentioned in MATERIALS AND METHODS, on the time scale shown, the Ca^{2+}-ATP reaction is virtually in kinetic equilibrium with Δ[Ca^{2+}], and (*b*) since the effective value of ATP's $K_{d,Ca}$ is large (2.2 mM; Table I), the Ca^{2+}-ATP reaction deviates by <10% from linearity even for Ca^{2+} transients as large as 100 μM (the amplitude of Δ[Ca^{2+}] in the outer-most compartment nearest the Z line in the calculation of Fig. 4; not shown). Hence, the Δ[Ca^{2+}] changes for all compartments can be closely approximated from the Δ[CaATP] changes in Fig. 4 *C* if the latter are scaled by the factor 1/3.6 (see MATERIALS AND METHODS). Similarly, spatially averaged Δ[CaATP] can be closely approximated from the spatially averaged Δ[Ca^{2+}] waveform shown in Fig. 4 *A* if scaled by the factor 3.6. For spatially averaged Δ[CaATP], the actual values of peak amplitude, time-to-peak, and half-width are 63.7 μM, 3.2 ms, and 5.3 ms, respectively.

The principal conclusion from the calculation of Fig. 4 is that, with ATP included as a diffusible Ca^{2+}-binding species, spatially averaged Δ[Ca^{2+}] is close to expectation if the value of *R* in Eq. 3 is ~140 μM/ms. Based on (*a*) the fact that ATP is present in myoplasm at millimolar concentrations and presumably reacts with Ca^{2+} with reaction rate constants close to those listed in Table I, and (*b*) the finding of a great improvement in the agreement between calculated and measured Δ[Ca^{2+}] with inclusion of ATP in the multi-compartment model, two conclusions appear to be warranted. First, ATP likely plays an important role in the binding and transport of myoplasmic Ca^{2+}. Second, apart from a small time shift due to action potential propagation, the SR Ca^{2+} release function used in Fig. 4 is probably quite close to the actual SR Ca^{2+} release function of a small-diameter frog fiber.

As discussed in a later section of RESULTS, the need in Fig. 4 for an SR Ca^{2+} release function with an amplitude ~20% smaller than that estimated from the single-compartment model with ATP included reflects errors in the single-compartment model due to its inability to calculate effects of local saturation of Ca^{2+}-binding sites. The somewhat fortuitous result that the amplitude of the release function used in Fig. 4 (141 μM/ms) is very close to that estimated in the single-compartment calculation without ATP included (142 μM/ms; second section of RESULTS) is a related point that is also considered in a later section of RESULTS.

Role of ATP in Transporting Ca^{2+} within the Sarcomere

An additional feature of the calculation in Fig. 4 is that the diffusion of Ca^{2+} in the CaATP form is responsible for the spread of more total Ca^{2+} throughout the sarcomere than is the diffusion of free Ca^{2+}. This follows from the observation that, at any myoplasmic location, Δ[CaATP] is ~3.6-fold greater than Δ[Ca^{2+}], whereas the diffusion constant of free Ca^{2+} is only 2.1-fold greater than that of ATP (Table I). Thus, the flux of Ca^{2+} across compartment boundaries will be ~1.7-fold (= 3.6/2.1) greater for CaATP than for free Ca^{2+} (cf., Eq. 2).

To explore the importance of CaATP diffusion, it was of interest to repeat the multi-compartment calculation of Fig. 4 with the value of D_{ATP} reduced from 1.4×10^{-6} cm^2 s^{-1} to 0. In this circumstance, the spread of Ca^{2+} depends primarily on the diffusion of free Ca^{2+}. Fig. 5 shows the result, which reveals two significant points. First, a comparison of Figs. 5 *B* and 4 *B* shows that, with D_{ATP} reduced to 0, there is an increased occupancy of troponin with Ca^{2+} in the compartments nearest the Z line but a reduced occupancy in the compartments nearest the m-line, as well as a reduced rate of rise in the latter compartments. Thus, the transport of Ca^{2+} in the CaATP form that occurs if $D_{ATP} = 1.4 \times 10^{-6}$ cm^2 s^{-1} results in a Ca^{2+}-troponin occupancy that is more uniform and more synchronous. This presumably enables a more uniform and synchronous activation of fiber force.

Second, spatially averaged Δ[Ca^{2+}] in Fig. 5 *A* has a peak amplitude of 24.7 μM, a time-to-peak of 3.4 ms, and a half-width of 6.2 ms. Although these values are not markedly different from those in Fig. 4 *A* (18.0 μM, 3.2 ms, and 5.2 ms, respectively), they are substantially different from the values mentioned in the first multi-compartment calculations of RESULTS. In those calculations, with ATP omitted entirely, Δ[Ca^{2+}] had a peak amplitude of 58.0 μM, a time-to-peak of 3.2 ms, and a half-width of 3.6 ms. Because the value of *R* in Eq. 3 was essentially identical for that calculation and the calculation of Fig. 5 (142 vs. 141 μM/ms, respectively), it follows that ATP produces a much smaller and broader Ca^{2+} transient simply through its ability to bind Ca^{2+} during the rising phase of Δ[Ca^{2+}] and release it during the falling phase. Thus, independent of its ability to transport Ca^{2+}, ATP acts as an important "temporal filter" of Δ[Ca^{2+}].

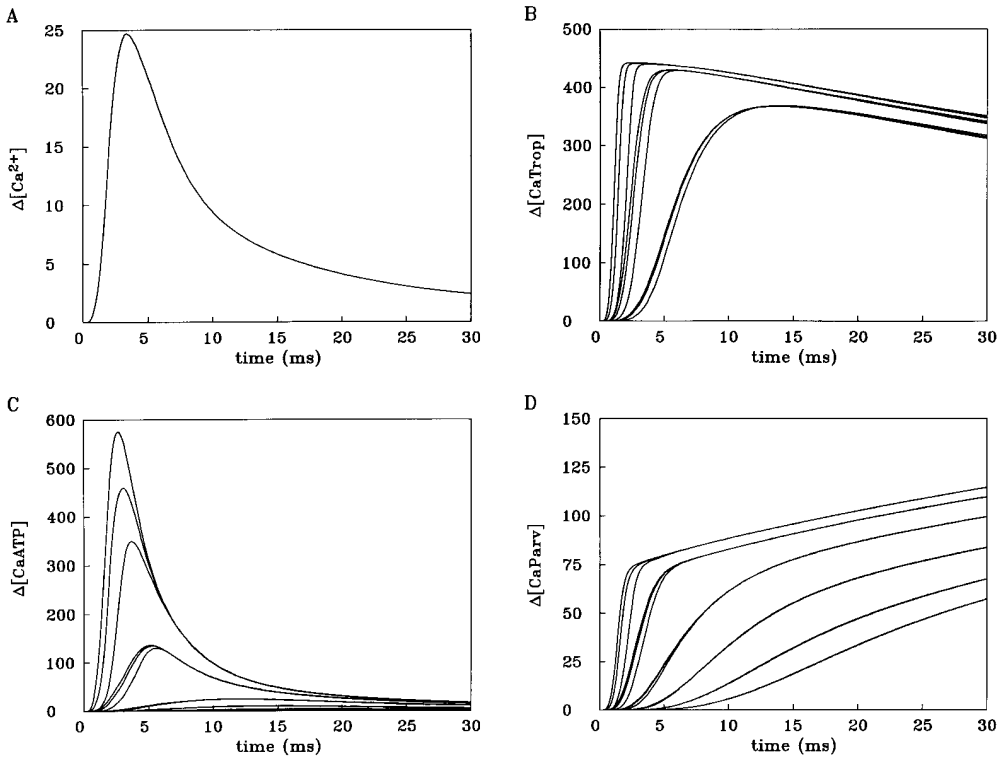

FIGURE 5. Multi-compartment calculation identical to that in Fig. 4, except that the diffusion constant of ATP was reduced from 1.4×10^{-6} $cm^2\ s^{-1}$ to 0.

Conclusions Based on an Examination of Changes to Other Parameters Listed in Table I

As described in the preceding sections, a significant binding and diffusive role for ATP is supported by the finding that inclusion of millimolar ATP in the model results in good agreement between the properties of calculated $\Delta[Ca^{2+}]$ and those extrapolated from the measurements of $\Delta[Ca^{2+}]$. A further test of the significance of this result is to examine whether, without ATP, adjustment of one or several of the many other parameters of the model listed in Table I might produce a comparable improvement in the properties of calculated $\Delta[Ca^{2+}]$. Although it was not possible to make an exhaustive exploration of all such model adjustments, several changes were investigated that, in the absence of ATP, were designed specifically to improve the agreement between calculated and measured $\Delta[Ca^{2+}]$. None of the changes was found to make the substantial qualitative difference that resulted from the inclusion of ATP. These other changes included (*a*) a threefold reduction in the peak rate of SR Ca^{2+} pumping (the parameter P in Eq. 4), (*b*) a twofold increase in the value of the diffusion constant of free Ca^{2+} (D_{Ca} in Table I), (*c*) a threefold increase in the Ca^{2+}-parvalbumin on-rate constant (k_{+1} for parvalbumin in Table I), and (*d*) use of a smaller and broader SR Ca^{2+}-release function. With changes *a–c*, whether implemented individually or simultaneously, there was no major improvement in the agreement between modeled and measured $\Delta[Ca^{2+}]$. With changes of type *d*, if sufficiently large, it was possible to produce a $\Delta[Ca^{2+}]$ with a peak amplitude of ~18 μM and a half-width of 5-6 ms, but these improvements were achieved only at the expense of the appearance of a slow foot on the rising phase of $\Delta[Ca^{2+}]$ and a delayed time-to-peak of $\Delta[Ca^{2+}]$ (~5 ms). In sum, the inability of these changes to produce an acceptable spatially averaged $\Delta[Ca^{2+}]$ further supports the idea that ATP does indeed contribute importantly to the determination of $\Delta[Ca^{2+}]$.

The Possible Importance of other Myoplasmic Ca^{2+}-binding Species

A related question is whether inclusion of other types of Ca^{2+}-binding species in the multi-compartment model can produce improvements similar to that produced by ATP. For example, some neuronal cells appear to contain substantial concentrations of a nondiffusible, low-affinity Ca^{2+} buffer(s), which may strongly influence $\Delta[Ca^{2+}]$ (Helmchen et al., 1996). This possibility was examined in our multi-compartment model by a comparison of the effects of such a hypothetical fixed buffer (HFB) with those of ATP. For these comparisons, HFB was assumed to be distributed in all myoplasmic compartments and have values of k_{+1} and k_{-1} identical to those listed in Table I for ATP. A further constraint for these calculations was that, for each concentration of HFB con-

sidered, the value of R (Eq. 3) was always adjusted so that the peak amplitude of $\Delta[Ca^{2+}]$ would be 18 μM.

The first calculation assumed that ATP was absent but that HFB was present at a concentration of 8 mM. This situation is similar to that shown in Fig. 5, except that a smaller value of R is used (118 μM/ms) so as to yield an 18 μM $\Delta[Ca^{2+}]$ transient. In this case, the values for time-to-peak and half-width of $\Delta[Ca^{2+}]$ are 3.4 and 5.4 ms, respectively, which are essentially identical to those in Fig. 4 *A* (3.2 and 5.2 ms, respectively). Thus, in terms of the ability to generate a satisfactory $\Delta[Ca^{2+}]$ response, the presence of HFB in the multi-compartment is very comparable to that of ATP. However, this calculation also reveals that, because of the inability of HFB to diffuse, there is substantially less occupancy of troponin with Ca^{2+} in the three troponin-containing compartments most distant from the Z line—on average, only 64% with HFB (vs. 86% with ATP; Fig. 4 *B*). As in Fig. 5, this calculation provides another demonstration of the importance of the diffusibility of a low-affinity buffer for achieving a high Ca^{2+}-occupancy of troponin all along the thin filament and indicates that the calculations with HFB alone are not as satisfactory as those with ATP alone.

The second calculations with HFB assumed that ATP was present in the usual amount (8 mM) and examined how the presence of different concentrations of HFB affected the time course of $\Delta[Ca^{2+}]$. The first such calculation assumed a concentration of HFB equal to that of ATP, 8 mM. In this case, the required value of R for an 18 μM $\Delta[Ca^{2+}]$ was 171 μM/ms, and the time-to-peak and half-width of $\Delta[Ca^{2+}]$ were 3.6 and 9.9 ms, respectively. Since the value for half-width is substantially longer than expected (~6 ms), it seems unlikely, given that skeletal muscle contains ~8 mM ATP, that it also contains a similar or larger concentration of HFB.

The next step was to reduce the concentration of HFB to identify the value that would give a half-width for $\Delta[Ca^{2+}]$ of 6 ms, i.e., essentially that expected from the experimental measurements. This concentration was 1.8 mM (with associated value of R = 148 μM/ms), and the value for time-to-peak of $\Delta[Ca^{2+}]$ was 3.3 ms. Since the occupancy of troponin with Ca^{2+} in this calculation was also high in all of the troponin-containing compartments (>85%), the presence of this concentration of HFB in muscle seems plausible. Indeed, with 1.8 mM HFB, the time-to-peak and half-width of $\Delta[Ca^{2+}]$ are in better overall agreement with the values expected from the experimental measurements than is the $\Delta[Ca^{2+}]$ of Fig. 4 (time-to-peak, 3.2 ms; half-width, 5.2 ms).

In summary, these calculations indicate that it is unlikely that skeletal muscle contains a concentration of low-affinity fixed buffer (in ATP-equivalent units) as large as 10% of that postulated for nerve (Helmchen et al., 1996). However, the possibility that muscle contains a few percent of that postulated for nerve cannot be ruled out and, in fact, may be supported by the calculations.

A final calculation in this general category was to omit HFB entirely and identify what concentration of ATP alone would give values for peak and half-width of $\Delta[Ca^{2+}]$ that were essentially the same as noted in the preceding paragraphs with the inclusion of 1.8 mM HFB. (Again, a constraint for these calculations was that, for each concentration of ATP considered, the value of R was readjusted to give a peak amplitude of 18 μM for $\Delta[Ca^{2+}]$.) With 9.2 mM ATP and with an R of 148 μM/ms, the time-to-peak and half-width values of $\Delta[Ca^{2+}]$ are 3.3 and 6.0 ms, respectively. Thus, inclusion of ATP alone at 9.2 mM (rather than 8 mM) gives a calculated $\Delta[Ca^{2+}]$ that is virtually identical to that obtained with inclusion of 8 mM ATP and 1.8 mM HFB. As noted in MATERIALS AND METHODS, the concentration of phospho-creatine found in muscle, ~40 mM, approximates 2 mM of ATP-equivalent (diffusible) low-affinity Ca^{2+} buffer. Phospho-creatine thus provides a basis for a modest increase in the ATP-equivalent concentration used in the model.

In summary, the calculations of this section do not exclude, but also do not necessarily support, the presence of a small concentration of HFB in myoplasm. They do, however, argue against the likelihood of a concentration of HFB as large as 10% of that found in nerve.

Comparison of the Single-compartment Model without ATP and the Multi-compartment Model with ATP

In Fig. 4, the multi-compartment model with ATP was driven by an SR Ca^{2+} release function of amplitude 141 μM/ms, which is essentially identical to the 142 μM/ms value estimated from the single-compartment model without ATP (cf., Fig. 3). This similarity implies that the error in the single-compartment estimates of SR release associated with the omission of ATP are offset by other errors. Several factors appear to contribute to these other errors.

First, a single-compartment model does not consider separate myoplasmic regions with differing degrees of local saturation of binding sites. Thus, a single-compartment model will, for a given spatially averaged $\Delta[Ca^{2+}]$, maximize—and thus over-estimate—the amount of Ca^{2+} captured by the intrinsic buffer sites included in the model (which are assumed to react with Ca^{2+} with a 1:1 stoichiometry). Moreover, the erroneous extra Ca^{2+} that the single-compartment model assigns to binding by the intrinsic buffers occurs early in time, when the myoplasmic gradients in $[Ca^{2+}]$ (as estimated by the multi-compartment model) are large. For example, the multi-compartment model estimates that $\Delta[Ca^{2+}]$ in the compartments nearest the Z line rises rapidly to

~100 μM, and as a result, there is rapid, local saturation of the troponin sites in these regions (Fig. 4 *B*). In contrast, in the other compartments, significant diffusional delays affect the rise of Δ[CaTrop]. Thus, in the single-compartment model, both kinetic and steady-state errors arise from the spatially homogeneous estimation of Ca^{2+} binding to the intrinsic buffers.

Second, calculations with the multi-compartment model show that some local saturation of furaptra with Ca^{2+} also occurs at early times near the release sites (see next section). This local saturation results in an estimate of $\Delta[Ca^{2+}]$ from furaptra that has a later time-to-peak and broader half-width than does the actual $\Delta[Ca^{2+}]$. By itself, use of a delayed $\Delta[Ca^{2+}]$ to drive the single-compartment model will result in an estimate of SR Ca^{2+} release that is delayed with respect to the actual release waveform.

Third, because of the same early local saturation of furaptra, the amplitude of spatially averaged $\Delta[Ca^{2+}]$, if calibrated with the actual myoplasmic $K_{d,Ca}$ of the indicator, will be underestimated. As discussed earlier, a value of 98 μM was assumed for furaptra's $K_{d,Ca}$ so that the amplitude of $\Delta[Ca^{2+}]$ calibrated from the indicator's Δf_{CaD} would agree with $\Delta[Ca^{2+}]$ measured with PDAA. The next section shows that the 98 μM value is probably larger than the actual myoplasmic value, and its use in the single-compartment model partially compensates for the other errors that arise because of the local saturation of sites with Ca^{2+}.

Characterization of Probable Error in the Previous Estimate of Furaptra's $K_{d,Ca}$ and in the Single-compartment Estimates of SR Ca^{2+} Release

Fig. 6 shows several additional calculations associated with the multi-compartment model of Fig. 4. For these calculations, a nonperturbing concentration of furaptra (1 μM) was included as a separate Ca^{2+}-binding species in all compartments, and the diffusion constant of furaptra was assumed to be 0.68×10^{-6} cm^2 s^{-1} (Konishi et al., 1991). In Fig. 6 *A*, the continuous trace is identical to the spatially averaged $\Delta[Ca^{2+}]$ shown in Fig. 4 *A* (called here "true" spatially averaged $\Delta[Ca^{2+}]$, i.e., as calculated under the assumptions of the model). In Fig. 6 *B*, the spatially averaged Δf_{CaD} signal for furaptra was simulated by the multi-compartment model under two different assumptions about indicator properties. For both simulations, furaptra was assumed to have a value of k_{-1} (Scheme A) of 5,000 s^{-1} (Zhao et al., 1997). For the first calculation (Fig. 6 *B*, *dotted trace*), a value of 5.1×10^7 M^{-1} s^{-1} was assumed for k_{+1} (thus $K_{d,Ca}$ = 98 μM, as assumed by Konishi et al. [1991] and Zhao et al. [1996]); for the second calculation (Fig. 6 *B*, *dashed trace*), the k_{+1} value was 7.1×10^7 M^{-1} s^{-1} ($K_{d,Ca}$ = 70 μM). Fig. 6 *B* shows that, with a $K_{d,Ca}$ of 70 μM, the amplitude of Δf_{CaD} is significantly larger, 0.151 (vs. 0.120 if $K_{d,Ca}$ is 98 μM). The 0.151 value is essentially identical to the average value of 0.150 observed for Δf_{CaD} in the experiments on small-diameter frog fibers (described in the first section of RESULTS). Thus, the dotted trace in Fig. 6 *B* indicates that the peak of ~0.15 for furaptra's spatially averaged Δf_{CaD} signal cannot be explained under the assumptions that $K_{d,Ca}$ is 98 μM and that the peak of spatially averaged $\Delta[Ca^{2+}]$ is 18 μM. Since the peak of $\Delta[Ca^{2+}]$ is thought to be close to 18 μM, we conclude that furaptra's myoplasmic $K_{d,Ca}$ is likely to be closer to 70 μM than to 98 μM.

Considered as temporal waveforms, the two Δf_{CaD} responses in Fig. 6 *B* are essentially identical (times-to-peak, 3.8–3.9 ms; half-widths, 8.1–8.2 ms). Both times-to-peak are noticeably slower than the 3.2 ms time-to-peak of true spatially averaged $\Delta[Ca^{2+}]$ (Fig. 4 *A*, *continuous*

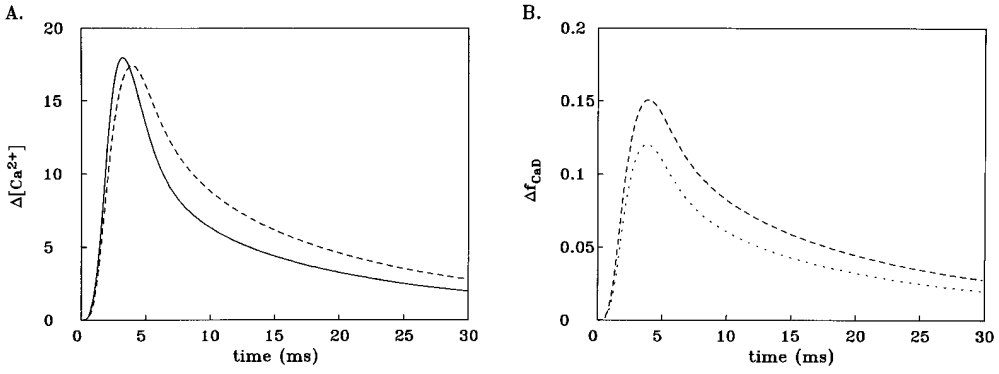

FIGURE 6. Multi-compartment simulations to illustrate the effects of local furaptra saturation on the estimation of furaptra's $\Delta[Ca^{2+}]$ by the single-compartment approach. The continuous trace in *A* is identical to that in Fig. 4 *A*, i.e., is "true" spatially averaged $\Delta[Ca^{2+}]$ as calculated by the multi-compartment model with ATP included. The traces in *B* represent two multi-compartment simulations of the spatially averaged furaptra Δf_{CaD} signal based on two assumed values for $K_{d,Ca}$ of the indicator in myoplasm (70 μM for the *dashed trace*, 98 μM for the *dotted trace*). For these calculations, a nonperturbing concentration of furaptra (1 μM) was included in each compartment in Fig. 1, but otherwise the simulation conditions were identical to those of Fig. 4. In *A*, the dashed trace is a single-compartment calculation of $\Delta[Ca^{2+}]$, which is based on the dashed trace in *B* and the assumption that $K_{d,Ca}$ is 98 μM.

trace). The delay in time-to-peak of Δf_{CaD} is due to local saturation of furaptra with Ca^{2+} because no such delay is found if Δf_{CaD} is driven by $\Delta[Ca^{2+}]$ in a single-compartment simulation (not shown).

The dashed trace in Fig. 6 *A* is a single-compartment calculation of spatially averaged $\Delta[Ca^{2+}]$ based on the dashed Δf_{CaD} response in Fig. 6 *B*; for this conversion, a furaptra $K_{d,Ca}$ of 98 μM was used, and the steady-state form of the 1:1 binding equation was assumed. This trace thus simulates previous experimental estimates of $\Delta[Ca^{2+}]$ based on a furaptra Δf_{CaD} signal of typical amplitude and the previously assumed value of $K_{d,Ca}$. In Fig. 6 *A*, the peak amplitudes of $\Delta[Ca^{2+}]$ are nearly identical (18 μM for the continuous trace, 17.5 μM for the dashed trace); this is expected since $K_{d,Ca}$ for furaptra was chosen previously to make the amplitude of furaptra's $\Delta[Ca^{2+}]$ agree with that of PDAA's (cf., first section of RESULTS). The time courses of the two changes in Fig. 6 *A*, however, are obviously different (time-to-peak of 3.2 ms and half-width of 5.2 ms for the continuous trace vs. 3.9 and 8.1 ms, respectively, for the dashed trace). As mentioned above, the fact that the time course of the simulated furaptra $\Delta[Ca^{2+}]$ is slower than that of true $\Delta[Ca^{2+}]$ reflects the effects of local saturation of the indicator with Ca^{2+}, which the single-compartment calculation cannot take into account. This error in time course would be smaller for an indicator of lower affinity, which would undergo less local saturation. Indeed, if calculations analogous to those of Fig. 6 are carried out with PDAA ($K_{d,Ca} \approx 1$ mM), the simulated peak amplitude of Δf_{CaD} is only 0.017, and the single-compartment conversion of Δf_{CaD} to spatially averaged $\Delta[Ca^{2+}]$ yields a peak amplitude of 17.3 μM, a time-to-peak of 3.3 ms, and a half-width of 5.4 ms (calculations not shown). As expected, these values are very close to those of true $\Delta[Ca^{2+}]$.

Since a number of previous publications, from this and other laboratories, have used a single-compartment model without ATP to estimate SR Ca^{2+} release parameters, it was of interest to use the multi-compartment model with ATP to characterize the likely errors in these estimates. Table II gives this information for estimates obtained with PDAA and furaptra. Column 1 (part *A* for $\Delta[Ca_T]$; part *B* for $d\Delta[Ca_T]/dt$) gives the information related to the release function used to drive the standard multi-compartment calculation with ATP (Fig. 4) and thus provides the "true" reference point for the comparisons in Table II. For the estimates in column 2, the dashed trace in Fig. 6 *A* was used as the $\Delta[Ca^{2+}]$ to drive the single-compartment model. (As mentioned above, this trace simulates a furaptra $\Delta[Ca^{2+}]$ signal, calibrated as in Fig. 3.) A comparison of column 2 with column 1 shows that, somewhat fortuitously, the single-compartment model without ATP provides generally accurate estimates of the true release parameters; the main error is a modest overestimation of the time-to-peak of release. Column 3 shows analogous release parameters based on use of the simulated PDAA $\Delta[Ca^{2+}]$ signal mentioned above. Again, the release parameters in column 3 are in reasonable agreement with those in column 1. Overall, the SR release parameters estimated from furaptra are in slightly better agreement with the true release parameters than are those from PDAA, even though there is more error in the single-compartment estimate of spatially averaged $\Delta[Ca^{2+}]$ with furaptra than with PDAA (see above and next section). This result, which is again somewhat fortuitous, indicates that the totality of errors inherent in the difference between the single-compartment model without ATP and the multi-compartment model with ATP (see preceding section) is offset slightly better with furaptra and its previous method of calibration ($K_{d,Ca} = 98$ μM) than with PDAA.

General Analysis of Errors in $\Delta[Ca^{2+}]$ Associated with Single-compartment Calculations

The preceding section compared single- and multi-compartment estimations of spatially averaged $\Delta[Ca^{2+}]$ from furaptra and PDAA and noted several sources of error inherent in the single-compartment estimates. This section further characterizes these errors by means of analogous calculations applied to a hypothetical family of indicators. For this analysis, all indicators are assumed to react with Ca^{2+} with an identical value of k_{+1}

TABLE II

SR Ca^{2+} Release Compared with Single- and Multi-compartment Models

	1	2	3
A. $\Delta[Ca_T]$			
Actual peak (μM)	296	—	—
Estimated peak (μM)	292	290	284
Time of estimated peak (ms)	5.8	6.1	5.3
B. $d\Delta[Ca_T]/dt$			
Peak (μM/ms)	141	141	153
Time-to-peak (ms)	1.70	2.07	2.00
Half-width (ms)	1.93	1.87	1.70

Column 1 refers to the multi-compartment model of Fig. 4, which includes ATP and is considered the reference point for the comparisons. Part *B* of column 1 gives the parameters of the release waveform used to drive this model. In part *A*, the "actual" peak is the value of this waveform integrated from time zero to infinity, whereas the "estimated" peak refers to the peak value of the waveform obtained as the sum of $\Delta[Ca^{2+}]$, Δ[CaTrop], Δ[CaParv], and, in the case of column 1, Δ[CaATP]. (These waveforms reach a peak and then decay because of SR Ca^{2+} pumping.) Columns 2 and 3 give release parameters as estimated by the single-compartment model without ATP if driven by the multi-compartment simulation of spatially averaged $\Delta[Ca^{2+}]$ (which was calculated for each of the indicators; see text). Column 2 is for a furaptra simulation (assumed $K_{d,Ca}$ of furaptra is 70 μM for the multi-compartment simulation and 98 μM for the single-compartment reestimation of $\Delta[Ca^{2+}]$; see RESULTS). Column 3 is analogous to column 2 but is for a PDAA simulation (assumed $K_{d,Ca}$ of PDAA, 1 mM for both parts of the simulation).

but with different values of k_{-1} and hence different values of $K_{d,Ca}$. The value selected for k_{+1}, 5×10^7 M^{-1} s^{-1}, lies in the range considered for furaptra in the previous section ($5–7 \times 10^7$ M^{-1} s^{-1}) and is probably also similar to that which applies to many members of the family of tetra-carboxylate Ca^{2+} indicators (cf., Tsien, 1980) when in the myoplasmic environment, e.g., indo-1, fura-2, fluo-3, calcium-orange-5N, etc. (Zhao et al., 1996). In general, these indicators bind heavily to myoplasmic constituents, and as a consequence, their rate constants for reaction with Ca^{2+} appear to be substantially reduced in comparison with those of the indicator in free solution. Six values of k_{-1} were selected for these calculations: 10^1 s^{-1}, 10^2 s^{-1},..., 10^6 s^{-1}, with the corresponding values of $K_{d,Ca}$ being 0.2 μM, 2 μM,..., 20 mM.

Fig. 7 (described in detail beginning with the next paragraph) summarizes the results of this analysis. As in the preceding section (cf., Fig. 6 and Table II), the multi-compartment model with ATP included is assumed to give the "true" results (Fig. 7, *B* and *D*, *horizontal dotted lines*) against which the simulated $\Delta[Ca^{2+}]$ from each of the indicators can be compared. To calculate an indicator's $\Delta[Ca^{2+}]$, the fraction of the indicator bound with Ca^{2+} (spatially averaged Δf_{CaD} plus the resting fraction, f_{CaD}; Fig. 7 *A*) was calculated by the multi-compartment model, based on a nonperturbing concentration of indicator (1 μM) included in all compartments. For simplicity, the myoplasmic diffusion constant of all indicators was fixed in the calculations at 0.25×10^{-6} cm^2 s^{-1} (cf., Zhao et al., 1996). For the conversion of an indicator's $f_{CaD} + \Delta f_{CaD}$ response to $\Delta[Ca^{2+}]$, two different single-compartment methods were used. In the first method (Fig. 7, *B* and *D*, *dashed curves*), $f_{CaD} + \Delta f_{CaD}$ was converted to $\Delta[Ca^{2+}]$ by the steady-state form of the 1:1 binding equation, i.e., as was done for the conversion of the dashed Δf_{CaD} curve in Fig. 6 *B* to the dashed $\Delta[Ca^{2+}]$ curve in Fig. 6 *A*. In the second method (Fig. 7, *B* and *D*, *continuous curves*; also traces in Fig. 7 *C*), the kinetic form of the 1:1 binding equation was used (see for example Baylor and Hollingworth, 1988; Klein et al., 1988; Hollingworth et al., 1992). Necessarily, the second method gives a $\Delta[Ca^{2+}]$ with a larger peak amplitude and a briefer half-width than does the first method. Even though the second approach partially compensates for the kinetic lag between $\Delta[Ca^{2+}]$ and Δf_{CaD} that arises when k_{-1} is small, this method cannot be expected to correct for errors related to gradients in indicator saturation.

In Fig. 7 *A*, six time-dependent calculations of $f_{CaD} + \Delta f_{CaD}$ are plotted, corresponding to the six different choices of k_{-1}. As k_{-1} increases from 10^1 s^{-1} to 10^6 s^{-1}, f_{CaD} becomes progressively smaller and Δf_{CaD} becomes

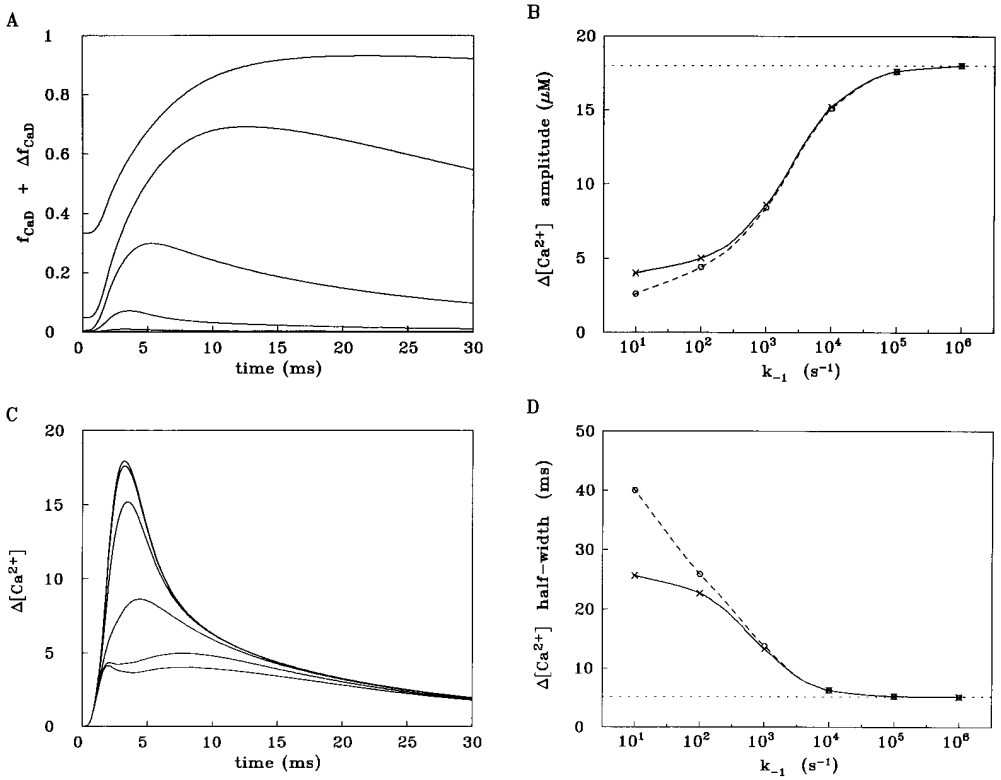

FIGURE 7. Analysis of responses of a hypothetical family of Ca^{2+} indicators assumed to react with Ca^{2+} with a fixed value of k_{+1} (5×10^7 M^{-1} s^{-1}) but with different values of k_{-1} (order of magnitude increases from 10^1 to 10^6 s^{-1}). All simulations started with the multi-compartment model with ATP, whereby "true" spatially averaged $\Delta[Ca^{2+}]$ and "true" spatially averaged Δf_{CaD} of the indicators were calculated. A single-compartment model was then used to convert Δf_{CaD} to $\Delta[Ca^{2+}]$ by one of two methods. The first approach (cf., *B* and *D*, *dashed curves*) used the steady-state form of the 1:1 binding equation. The second approach (cf., *B* and *D*, *continuous curves*) used the kinetic form of the same equation. *A* shows the calculation of $f_{CaD} + \Delta f_{CaD}$ for the six multi-compartment simulations, whereas *B* shows the amplitude of spatially averaged $\Delta[Ca^{2+}]$, as calculated from the $f_{CaD} + \Delta f_{CaD}$ signals in the two single-compartment approaches. *D* is similar to *B* except that the half-width of $\Delta[Ca^{2+}]$ is analyzed. *C* shows the spatially averaged $\Delta[Ca^{2+}]$ traces calculated from the traces in *A* by the kinetic form of the 1:1 binding equation.

both briefer and smaller. At the largest value of k_{-1}, both f_{CaD} and Δf_{CaD} are too small to be resolved above baseline at the gain shown. With the first (steady-state) method of conversion of the traces in Fig. 7 *A* to $\Delta[Ca^{2+}]$ ($\Delta[Ca^{2+}]$ traces not shown), values of k_{-1} approaching 10^5 s^{-1} or greater are required if both the peak amplitude and half-width of $\Delta[Ca^{2+}]$ (Fig. 7, *B* and *D*, respectively, *circle points connected by dashed curves*) are to agree well with those of true $\Delta[Ca^{2+}]$ (Fig. 7, *B* and *D*, *horizontal dotted lines*). With values of $k_{-1} \leq 10^4$ s^{-1}, a progressively larger disparity is observed between the parameters of calculated and true $\Delta[Ca^{2+}]$.

The traces in Fig. 7 *C* show the results of the second (kinetic) method of conversion of the traces in Fig. 7 *A* to $\Delta[Ca^{2+}]$ and were used to calculate the second set of points in Fig. 7, *B* and *D* (*cross points connected by continuous curves*). As mentioned above, $\Delta[Ca^{2+}]$ parameters are necessarily larger and briefer with this method and thus the continuous curves in Fig. 7, *B* and *D*, lie closer to the horizontal dotted lines than do the dashed curves. Interestingly, with this method of conversion, $\Delta[Ca^{2+}]$ in Fig. 7 *C* becomes obviously biphasic at the two smallest values of k_{-1} (10^1 s^{-1} and 10^2 s^{-1}), and at the next larger value of k_{-1} (10^3 s^{-1}), a hump can be seen on the rising phase of $\Delta[Ca^{2+}]$. The appearance of two phases in $\Delta[Ca^{2+}]$ is an artifact of local indicator saturation in combination with the use of a single-compartment kinetic correction to convert the $f_{CaD} + \Delta f_{CaD}$ response to $\Delta[Ca^{2+}]$. The earlier phase, which rises to a plateau during the time of SR Ca^{2+} release, reflects effects of indicator saturation at sarcomeric regions close to the release sites. The later phase, which involves a delay in the rise of $\Delta[Ca^{2+}]$ and Δf_{CaD} at sarcomeric locations more distant from the release sites, reflects the time required for Ca^{2+} to diffuse and bind to indicator in these locations. (Note: The biphasic response does not depend on the diffusion of indicator since it is also seen if the diffusion constant of the indicator is set to zero in the multi-compartment part of the calculation; not shown.)

Overall, the simulations in Fig. 7 indicate that, at values of $k_{-1} < 10^4$ s^{-1}, effects due to Ca^{2+} gradients and local saturation of indicator introduce significant error in single-compartment methods for estimation of true $\Delta[Ca^{2+}]$. Moreover, at $k_{-1} \leq 10^3$ s^{-1}, these errors are quite severe. Thus, this analysis supports the conclusion that, to achieve an accurate estimate of true $\Delta[Ca^{2+}]$ in spatially averaged measurements, it is highly desirable to use a low-affinity, rapidly responding indicator (Hirota et al., 1989).

Application of the Multi-compartment Model to Reestimate Myoplasmic Values of the Ca^{2+}-fluo-3 Reaction Rates

Previous publications from this and other laboratories (e.g., Baylor and Hollingworth, 1985, 1988; Klein et al., 1988; Harkins et al., 1993; Kurebayashi et al., 1993; Pape et al., 1993; Westerblad and Allen, 1996; Zhao et al., 1996) have described single-compartment methods for estimation of Ca^{2+} reaction rates (k_{+1} and k_{-1}) of a number of different indicators when in the myoplasmic environment. In the most common type of experiment, the same region of the same fiber was exposed to two indicators—usually a lower-affinity indicator (e.g., antipyrylazo III, furaptra, or PDAA) and a higher-affinity indicator (e.g., fura-2, fura-red, or fluo-3)—and optical measurements were made simultaneously from both indicators. The optical responses from the lower-affinity indicators (whether recorded in the same or different fibers) were usually very similar in time course, whereas the responses from the higher-affinity indicators, while somewhat variable in time course, always had significantly later times-to-peak and broader half-widths than did the lower-affinity responses. The slower responses of the higher-affinity indicators were assumed to reflect the smaller values of k_{-1} that are inherent in these indicators being of higher-affinity, and the timing of these responses relative to the lower-affinity responses was used in single-compartment fits to estimate the values of k_{-1} and k_{+1} of the higher-affinity indicators. The results presented in the previous two sections, however, indicate that because of the effects of local indicator saturation, use of the single-compartment method will probably introduce significant error in the estimates of k_{-1} and k_{+1}. It was therefore of interest to use the multi-compartment model to reestimate k_{-1} and k_{+1} values for one of the higher-affinity indicators, as a means of assessing the direction and magnitude of possible errors in the previous estimates.

The indicator selected for this analysis was fluo-3, which has been used in a number of recent measurements of local Ca^{2+} signals in muscle (e.g., Cheng et al., 1993; Tsugorka et al., 1995; Klein et al., 1996; Hollingworth et al., 1998). Results with the multi-compartment model were compared with the traces and single-compartment analysis of Harkins et al. (1993; cf., their Fig. 8). These authors reported average values for k_{+1} and k_{-1} of fluo-3 of 1.31×10^7 M^{-1} s^{-1} and 33.5 s^{-1}, respectively (16°C), with the corresponding value of $K_{d,Ca}$ being 2.56 μM. If these values are used in a multi-compartment calculation of the type shown in Fig. 6, a poor fit of the simulated data of Harkins et al. (1993) is obtained (not shown). Additional calculations were therefore carried out with the multi-compartment model to find values of k_{+1} and k_{-1} that gave a better fit to these data. A good fit was obtained with k_{+1} and k_{-1} values of 3.5×10^7 M^{-1} s^{-1} and 55 s^{-1}, respectively ($K_{d,Ca}$ of 1.57 μM). We conclude that the new estimates of k_{+1} and k_{-1} are probably closer to the actual rates that apply to fluo-3 in myoplasm and that the use of a single-compartment method probably underestimates the actual rates of

higher-affinity indicators. Although the new estimates for fluo-3 are significantly larger than the previous estimates, they are still markedly smaller than the rates reported for the indicator in a simple salt solution ($\sim 8 \times 10^8$ M^{-1} s^{-1} and ~ 400 s^{-1} at 22°C and a viscosity of 1 cP; Eberhard and Erne, 1989; Lattanzio and Bartschat, 1991).

DISCUSSION

A Multi-compartment Model That Includes Ca^{2+}-binding to ATP and Diffusion of CaATP

In this article, we describe a multi-compartment model of a half-sarcomere that calculates the spread of Ca^{2+} within a single myofibril of a frog twitch fiber. This model is similar to that first developed by Cannell and Allen (1994) but incorporates several important changes that reflect current knowledge of the Ca^{2+} release process and the myoplasmic environment. These changes include a smaller value for the diffusion constant of free Ca^{2+}, a larger and briefer SR Ca^{2+} release event in response to an action potential, and the inclusion of ATP as a diffusible species that binds both Ca^{2+} and Mg^{2+}. As shown in MATERIALS AND METHODS, at the free Mg^{2+} concentration of myoplasm ($\sim$1 mM), ATP behaves as a low-affinity, rapidly reacting Ca^{2+} buffer. Additionally, ATP (mol wt 507) has a diffusion constant in myoplasm ($\sim 1.4 \times 10^{-6}$ cm^2 s^{-1}; 16°C) that is about half that of Ca^{2+} (Kushmerick and Podolsky, 1969). Thus, there should be a significant transport of Ca^{2+} along the sarcomere in the CaATP form. Probably the most important result of our modeling is that, without ATP (or an analogous compound), the measurements of spatially averaged $\Delta[Ca^{2+}]$ in frog fibers could not be adequately simulated with the SR Ca^{2+} release function that is thought to result from a single action potential (peak amplitude of $\sim$140 μM/ms, half-width of $\sim$2 ms). Thus, our calculations (*a*) implicate the presence of a significant concentration of a low-affinity, rapidly reacting Ca^{2+}-binding species in myoplasm, and (*b*) show that ATP, with properties as reported in the biochemical and physiological literature, satisfies the requirements of this species. Since ATP is present in myoplasm at millimolar concentrations, is mobile, and is capable of binding Ca^{2+}, it seems hard to avoid the conclusion that ATP plays a role similar to that inferred with our model. It is possible, of course, that other compounds, both mobile (e.g., phospho-creatine) and immobile (cf., Helmchen et al., 1996), also contribute to the effects that our model assigns to ATP. However, the contribution of these other compounds appears to be minor in comparison with that of ATP.

Other Implications of the Presence of ATP in the Model

The calculation in Fig. 2 shows that Δ[CaATP] is expected to be three to four times larger than, and nearly in kinetic equilibrium with, $\Delta[Ca^{2+}]$. Since the diffusion constant of ATP is about half that of free Ca^{2+} (Table I), it follows that more Ca^{2+} diffuses within myoplasm as CaATP than as free Ca^{2+}. As shown by the comparison between Figs. 4 *B* and 5 *B*, the diffusion of CaATP helps synchronize the Ca^{2+}-occupancy of troponin and thus activation of the myofilaments.

Given that the peak value of spatially averaged Δ[CaATP] is $\sim$65 μM, the question arises whether the presence of ATP requires that SR Ca^{2+} release be $\sim$65 μM larger than it would otherwise be if ATP were not present (or did not bind Ca^{2+}). However, calculations (not shown) indicate that, to achieve a given high-level occupancy of the troponin regulatory sites, the amount of extra SR Ca^{2+} that must be released due to the presence of 8 mM ATP is only about 30 μM ($\sim$270 μM in the absence of ATP vs. $\sim$300 μM in the presence of ATP). The difference between 65 and 30 μM reflects the fact that Ca^{2+} quickly dissociates from ATP when $\Delta[Ca^{2+}]$ declines (cf., Figs. 2 and 4). Thus, Ca^{2+} from ATP is made available to bind to the troponin (and other) sites. Since the multi-compartment model indicates that slightly more than half of the Ca^{2+} that is bound by ATP is subsequently bound by troponin, the extra load that ATP adds to the SR release requirement is only $\sim$10%. For comparison, the increase in load due to the presence of parvalbumin is $\sim$20%. This follows from the observations that spatially averaged Δ[CaParv] also rises rapidly to about 65 μM but that the rate of Ca^{2+} dissociation from parvalbumin is very slow (cf., Table I). Thus, Ca^{2+} cannot dissociate from parvalbumin and be bound by troponin on the time scale of twitch activation.

Other Comparisons between the Single- and Multi-compartment Models

We were initially surprised that the estimate of SR Ca^{2+} release from the single-compartment model without ATP included supplied a satisfactory driving function for the multi-compartment model with ATP included. As considered in RESULTS, there appear to be several sources of offsetting error in the single-compartment model that account for this situation. As shown by the comparisons in Table II, the overall effect of these errors is offset slightly better in the case of $\Delta[Ca^{2+}]$ measurements with furaptra (if calibrated with a $K_{d,Ca}$ of 98 μM) than with PDAA, even though PDAA is thought to give a more reliable estimate of the actual time course of spatially averaged $\Delta[Ca^{2+}]$.

Based on our multi-compartment model, we have reanalyzed the data reported by Harkins et al. (1993), who estimated the values of k_{+1} and k_{-1} for the Ca^{2+}–fluo-3 reaction in myoplasm. While their reaction rates provide a useful empirical way to relate, in a single-compartment calculation, the Δf_{CaD} signal of fluo-3 to the

$\Delta[Ca^{2+}]$ signal of furaptra (calibrated by the method of Konishi et al., 1991), these rates may not accurately reflect fluo-3's actual myoplasmic values of k_{+1} and k_{-1}. Indeed, our multi-compartment model indicates that because of local saturation of the indicator with Ca^{2+} near the SR release sites, there is likely to be error in the previous single-compartment analysis (as well as in comparable analyses reported elsewhere in the literature for other indicators—see RESULTS). The new values that we estimate for fluo-3's k_{+1} and k_{-1} are 2.7- and 1.6-fold higher, respectively, than the rates reported by Harkins et al. (1993). It should be noted, however, that in our multi-compartment model of the half-sarcomere, Ca^{2+} enters the myoplasm only at the outermost compartment nearest the Z line, whereas in reality, some Ca^{2+} may enter a myofibril from adjacent myofibrils and/or SR release sites that are not in registration with the Z line. Thus, the local $\Delta[Ca^{2+}]$ gradients calculated by our model should probably be regarded as upper limits of the actual gradients. In support of this conclusion, our previous experiments with PDAA and furaptra (e.g., Fig. 6 *B* of Konishi et al., 1991) indicate that the difference between the time courses of spatially averaged $\Delta[Ca^{2+}]$ measured with these two indicators is slightly less extreme than calculated by our multi-compartment model (Figs. 6 *A* and 7 *D*). This, in turn, suggests that the k_{+1} and k_{-1} values estimated for fluo-3 by the multi-compartment model may slightly overestimate the actual Ca^{2+}–fluo-3 reaction rates in myoplasm.

Local indicator saturation probably also explains a finding reported by Pape et al. (1993), who used a single-compartment approach to estimate the value of k_{+1} for fura-2 in the myoplasm of cut fibers from spatially averaged PDAA and fura-2 measurements. They found that the estimate of k_{+1} varied with indicator concentration, increasing about twofold, from 3.5×10^7 M^{-1} s^{-1} to 7×10^7 M^{-1} s^{-1}, as myoplasmic [fura-2] rose from 0.5 to 2 mM. Since the spatially averaged $\Delta[Ca^{2+}]$ signal in these experiments was relatively large at a [fura-2] of 0.5 mM but nearly eliminated at a [fura-2] of 2 mM, it is possible that the estimate of k_{+1} increased because local saturation of fura-2 with Ca^{2+} was substantially reduced at the higher fura-2 concentrations. This interpretation is supported by calculations (not shown) carried out with our multi-compartment model, which were designed to simulate the experiment of Pape et al. (1993). In these simulations, the estimate of k_{+1} also increased twofold as the fura-2 concentration was increased from 0.5 to 2 mM. (Note: The value of k_{+1} estimated for fura-2 in cut fibers is severalfold larger than the value of k_{+1} estimated for fluo-3 in intact fibers [cf., last section of RESULTS]. Two effects probably underlie this difference. First, the binding of indicator to myoplasmic constituents has been associated with reductions in the values of indicator reaction rates, and fluo-3 appears to be more heavily bound in myoplasm than fura-2 [intact fiber measurements, summarized in Zhao et al., 1996]. Second, cut fibers appear to be ~40% more hydrated than intact fibers [as judged by measurements of intrinsic birefringence; Irving et al., 1987]. Therefore, reaction rates, may, in general, be higher in cut compared with intact fibers.)

A related point concerns previous estimations of the resting level of myoplasmic $[Ca^{2+}]$ ($[Ca^{2+}]_R$) with high-affinity indicators such as fluo-3 or fura-2. Often, the value estimated for $[Ca^{2+}]_R$ depends directly on an associated estimate of the myoplasmic value of the indicator's $K_{d,Ca}$. If $K_{d,Ca}$ is obtained from kinetic fits of spatially averaged measurements with two Ca^{2+} indicators, the multi-compartment calculations indicate that the value of $K_{d,Ca}$ is probably overestimated. For example, with fluo-3, our multi-compartment analysis implies that $K_{d,Ca}$ for fluo-3 lies closer to 1.6 μM than to the 2.6 μM value estimated by Harkins et al. (1993). Corrected for this error, the fluo-3 data of Harkins et al. imply a narrower range of estimates for $[Ca^{2+}]_R$, 0.10–0.14 μM rather than 0.10–0.24 μM. This correction helps slightly to reconcile the ~10-fold difference for $[Ca^{2+}]_R$ (0.03–0.3 μM) reported in skeletal muscle with different techniques (cf., Baylor et al., 1994; Westerblad and Allen, 1994).

Generalizations and Speculations

Since ATP is present in most cells at millimolar concentrations, it seems likely that the significant effects of ATP deduced here on the shaping of local Ca^{2+} gradients also applies to the many other cell types that use $\Delta[Ca^{2+}]$ to control their activity. For example, in secretory cells, the binding of Ca^{2+} by ATP and the diffusion of CaATP likely modify the amplitude and time course of the local $\Delta[Ca^{2+}]$ signals that control vesicle release.

A final speculation relates to the possibility that Δ[CaATP] might itself serve as an intracellular signal. Since the value of $K_{d,Ca}$ of ATP is large relative to $\Delta[Ca^{2+}]$, Δ[CaATP] provides a rapid, local monitor of the product of $\Delta[Ca^{2+}]$ and total [ATP]. Thus, a large Δ[CaATP] indicates both a substantial $\Delta[Ca^{2+}]$ and a substantial total [ATP]. This signal might be used by the cell to activate novel regulatory pathways.

We thank Dr. W.K. Chandler for helpful comments on the manuscript.

This work was supported by a grant from the U.S. National Institutes of Health (NS 17620) and the Muscular Dystrophy Association.

Original version received 8 May 1998 and accepted version received 29 June 1998.

REFERENCES

Adrian, R.H., and L.D. Peachey. 1973. Reconstruction of the action potential of frog sartorius muscle. *J. Physiol. (Camb.).* 235:103–131.

Baylor, S.M., W.K. Chandler, and M.W. Marshall. 1983. Sarcoplasmic reticulum calcium release in frog skeletal muscle fibres estimated from arsenazo III calcium transients. *J. Physiol. (Camb.).* 344:625–666.

Baylor, S.M., A.B. Harkins, and N. Kurebayashi. 1994. Response to Westerblad and Allen. *Biophys. J.* 66:927–928.

Baylor, S.M., and S. Hollingworth. 1988. Fura2 calcium transients in frog skeletal muscle fibres. *J. Physiol. (Camb.).* 403:151–192.

Baylor, S.M., and S. Hollingworth. 1998. The transient binding of calcium to ATP and diffusion of Ca-ATP help shape the amplitude and time course of the myoplasmic free Ca transient (Δ[Ca]). *Biophys. J.* 74:A235.

Baylor, S.M., S. Hollingworth, C.S. Hui, and M.E. Quinta-Ferreira. 1985. Calcium transients from intact frog skeletal muscle fibers simultaneously injected with antipyrylazo III and azo 1. *J. Physiol. (Camb.).* 365:70.

Baylor, S.M., M.E. Quinta-Ferreira, and C.S. Hui. 1985. Isotropic components of antipyryl-azo III signals from frog skeletal muscle fibers. *In* Calcium and Biological Systems. R.P. Rubin, G. Weiss, and J.W. Putney, Jr., editors. Plenum Publishing Corp., New York. 339–349.

Botts, J., A. Chashin, and H.L. Young. 1965. Alkali metal binding by ethylenediamine-tetraacetate, adenosine 5'-triphosphate, and pyrophosphate. *Biochemistry.* 4:1788–1796.

Cannell, M.B., and D.G. Allen. 1984. Model of calcium movements during activation in the sarcomere of frog skeletal muscle. *Biophys. J.* 45:913–925.

Cheng, H., W.J. Lederer, and M.B. Cannell. 1993. Calcium sparks: elementary events underlying excitation-contraction coupling in heart muscle. *Science.* 262:740–745.

Eberhard, M., and P. Erne. 1989. Kinetics of calcium binding to fluo-3 determined by stopped-flow fluorescence. *Biochem. Biophys. Res. Commun.* 163:309–314.

Eigen, M., and R.G. Wilkins. 1965. The kinetics and mechanism of formation of metal complexes. *In* Mechanisms of Inorganic Reactions, Advanced Chemistry Series. 49:55–67.

Escobar, A.L., J.R. Monk, J.M. Fernandez, and J.L. Vergara. 1994. Localisation of the site of Ca^{2+} release at the level of a single sarcomere in skeletal muscle fibers. *Nature.* 367:739–741.

Fernandez-Belda, F., M. Kurzmack, and G. Inesi. 1984. A comparative study of calcium transients by isotopic tracer, metallochromic indicator, and intrinsic fluorescence in sarcoplasmic reticulum ATPase. *J. Biol. Chem.* 259:9687–9698.

Franzini-Armstrong, C. 1975. Membrane particles and transmission at the triad. *Fed. Proc.* 34:1382–1389.

Gillis, J.M., D. Thomason, J. Lefevre, and R.H. Kretsinger. 1982. Parvalbumins and muscle relaxation: a computer simulation study. *J. Muscle Res. Cell Motil.* 3:377–398.

Godt, R.E., and D.W. Maughan. 1988. On the composition of the cytosol of relaxed skeletal muscle of the frog. *Am. J. Physiol.* 254: C591–C604.

Gordon, A.M., A.F. Huxley, and F.J. Julian. 1964. The length-tension diagram of single vertebrate striated muscle fibres. *J. Physiol.* 171:28–30.

Harkins, A.B., N. Kurebayashi, and S.M. Baylor. 1993. Resting myoplasmic free calcium in frog skeletal muscle fibers estimated with fluo-3. *Biophys. J.* 65:865–881.

Helmchen, F., K. Imoto, and B. Sakmann. 1996. Ca^{2+} buffering and action potential-evoked Ca^{2+} signaling in dendrites of pyramical neurons. *Biophys. J.* 70:1069–1081.

Hirota, A., W.K. Chandler, P.L. Southwick, and A.S. Waggoner. 1989. Calcium signals recorded from two new purpurate indicators inside frog cut twitch fibers. *J. Gen. Physiol.* 94:597–631.

Hollingworth, S., A.B. Harkins, N. Kurebayashi, M. Konishi, and S.M. Baylor. 1992. Excitation-contraction coupling in intact frog skeletal muscle fibers injected with mmolar concentrations of fura2. *Biophys. J.* 63:224–234.

Hollingworth, S., C. Soeller, S.M. Baylor, and M.B. Cannell. 1998. Local calcium gradients during activation of frog skeletal muscle measured with Mg-Green and Fluo-3. *Biophys. J.* 74:A235.

Hollingworth, S., M. Zhao, and S.M. Baylor. 1996. The amplitude and time course of the myoplasmic free $[Ca^{2+}]$ transient in fast-twitch fibers of mouse muscle. *J. Gen. Physiol.* 108:455–469.

Hou, T.-T., J.D. Johnson, and J.A. Rall. 1991. Parvalbumin content and Ca^{2+} and Mg^{2+} dissociation rates correlated with changes in relaxation rate of frog muscle fibres. *J. Physiol. (Camb.).* 441:285–304.

Irving, M., J. Maylie, N.L. Sizto, and W.K. Chandler. 1987. Intrinsic optical and passive electrical properties of cut frog twitch fibers. *J. Gen. Physiol.* 89:1–40.

Johnson, J.D., D.E. Robinson, S.P. Robertson, A. Schwartz, and J.D. Potter. 1981. Ca^{2+} exchange with troponin and the regulation of muscle contraction. *In* Regulation of Muscle Contraction: Excitation-Contraction Coupling. A.D. Grinnell and Mary A.B. Brazier, editors. Academic Press, New York. 241–259.

Jong, D.-S., P. Pape, S.M. Baylor, and W.K. Chandler. 1995. Calcium inactivation of calcium release in frog cut muscle fibers that contain millimolar EGTA or Fura-2. *J. Gen. Physiol.* 106:337–388.

Kargacin, M.E., and G.J. Kargacin. 1997. Predicted changes in concentrations of free and bound ATP and ADP during intracellular Ca^{2+} signaling. *Am. J. Physiol.* 273:C1416–C1426.

Klein, M.G., H. Cheng, L.F. Santana, Y.-H. Jiang, W J. Lederer, and M.F. Schneider. 1996. Two mechanisms of quantized calcium release in skeletal muscle. *Nature.* 379:455–458.

Klein, M.G., B.J. Simon, G. Szucs, and M.F. Schneider. 1988. Simultaneous recording of calcium transients in skeletal muscle using high and low affinity calcium indicators. *Biophys. J.* 53:971–988.

Konishi, M., and S.M. Baylor. 1991. Myoplasmic calcium transients monitored with purpurate indicator dyes injected into intact frog skeletal muscle fibers. *J. Gen. Physiol.* 97:245–270.

Konishi, M., S. Hollingworth, A.B. Harkins, and S.M. Baylor. 1991. Myoplasmic calcium transients in intact frog skeletal muscle fibers monitored with the fluorescent indicator furaptra. *J. Gen. Physiol.* 97:271–301.

Kurebayashi, N., A.B. Harkins, and S.M. Baylor. 1993. Use of fura red as an intracellular calcium indicator in frog skeletal muscle fibers. *Biophys. J.* 64:1934–1960.

Kushmerick, M.J. 1985. Patterns in mammalian muscle energetics. *J. Exp. Biol.* 115:165–177.

Kushmerick, M.J., and R.J. Podolsky. 1969. Ionic mobility in muscle cells. *Science.* 166:1297–1298.

Lattanzio, F.A., and D.K. Bartschat. 1991. The effect of pH on rate constants, ion selectivity and thermodynamic properties of fluorescent calcium and magnesium indicators. *Biochem. Biophys. Res. Commun.* 177:184–191.

Lenz, G.R., and A.E. Martell. 1964. Metal complexes of carnosine. *Biochemistry.* 3:750–753.

Martell, A.E., and R.M. Smith. 1974. Critical Stability Constants, Vol. 2. Plenum Publishing Corp., New York.

Maylie, J., M. Irving, N.L. Sizto, G. Boyarsky, and W.K. Chandler. 1987*a*. Calcium signals recorded from cut frog twitch fibers containing tetramethyl-murexide. *J. Gen. Physiol.* 89:145–176.

Maylie, J., M. Irving, N.L. Sizto, and W.K. Chandler. 1987*b*. Calcium signals recorded from cut frog twitch fibers containing antipyrylazo III. *J. Gen. Physiol.* 89:831–843.

Maylie, J., M. Irving, N.L. Sizto, and W.K. Chandler. 1987*c*. Comparison of Arsenazo III optical signals in intact and cut frog twitch fibers. *J. Gen. Physiol.* 89:41–81.

Nakajima, S., and A. Gilai. 1980. Radial propagation of muscle action potential along the tubular system examined by potential sensitive dyes. *J. Gen. Physiol.* 76:751–762.

Ogawa, Y., and M. Tanokura. 1986. Kinetic studies of calcium binding to parvalbumins from bullfrog skeletal muscle. *J. Biochem.* 99:81–89.

O'Sullivan, W.J., and D.D. Perrin. 1964. The stability constants of metal-adenine nucleotide complexes. *Biochemistry.* 3:18–26

Page, S.G., and H.E. Huxley. 1963. Filament lengths in striated muscle. *J. Cell Biol.* 19:369–390.

Pape, P.C., D.-S. Jong, W.K. Chandler, and S.M. Baylor. 1993. Effect of fura-2 on action potential–stimulated calcium release in cut twitch fibers from frog muscle. *J. Gen. Physiol.* 102:295–332.

Pape, P.C., M. Konishi, S. Hollingworth, and S.M. Baylor. 1990. Perturbation of sarcoplasmic reticulum calcium release and phenol red absorbance transients by large concentrations of fura-2 injected into frog skeletal muscle fibers. *J. Gen. Physiol.* 96:493–516.

Peachey, L.D. 1965. The sarcoplasmic reticulum and T-tubules of the frog's sartorius. *J. Cell Biol.* 25:209–231.

Phillips, R.C., P. George, and R.J. Rutman. 1966. Thermodynamic studies of the formation and ionization of the magnesium (II) complexes of ADP and ATP over the pH range 5 to 9. *J. Am. Chem. Soc.* 88:2631–2640.

Raju, B., E. Murphy, L.A. Levy, R.D. Hall, and R.E. London. 1989. A fluorescent indicator for measuring cytosolic free magnesium. *Am. J. Physiol.* 256:C540–C548.

Schneider, M.F., and B.J. Simon. 1988. Inactivation of calcium release from the sarcoplasmic reticulum in frog skeletal muscle. *J. Physiol. (Camb.).* 405:727–745.

Sillen, L.G., and A.E. Martell. 1964. Stability Constants of Metal Ion Complexes, 2nd ed. Special Publication No. 17, The Chemical Society, Burlington House, London.

Smith, R.M., and R.A. Alberty. 1956. The apparent stability constants of ionic complexes of various adenosine phosphates with divalent cations. *J. Am. Chem. Soc.* 78:2376–2380.

Southwick, P.L., and A.S. Waggoner. 1989. Synthesis of purpurate-1,1′-diacetic acid (PDAA) tri-potassium salt. A new calcium indicator for biological applications. *Org. Prep. Proc. Int.* 21:493–500.

Thompson, L.V., and R.H. Fitts. 1992. Muscle fatigue in the frog semitendinosus: role of the high-energy phosphates and P_i. *Am. J. Physiol.* 263:C803–C809.

Tsien, R.Y. 1980. New calcium indicators and buffers with high selectivity against magnesium and protons: design, synthesis, and properties of prototype structures. *Biochemistry.* 19:2396–2404.

Tsugorka, A., E. Rios, and L.A. Blatter. 1995. Imaging elementary events of calcium release in skeletal muscle cells. *Science.* 269: 1723–1726.

Westerblad, H., and D.G. Allen. 1994. Methods for calibration of fluorescent calcium indicators in skeletal muscle fibers. *Biophys. J.* 66:926–927.

Westerblad, H., and D.G. Allen. 1996. Intracellular calibration of the calcium indicator indo-1 in isolated fibers of *Xenopus* muscle. *Biophys. J.* 71:908–917.

Zhao, M., S. Hollingworth, and S.M. Baylor. 1996. Properties of tri- and tetra-carboxylate Ca^{2+} indicators in frog skeletal muscle fibers. *Biophys. J.* 70:896–916.

Zhou, Z., and E. Neher. 1993. Mobile and immobile calcium buffers in bovine adrenal chromaffin cells. *J. Physiol.* 469:245–273.